

# Minority Takeover in Majority Dynamics: Searching for Rare Initializations via the History Passing Algorithm

Marek Jankola<sup>a</sup>, Freya Behrens<sup>b</sup>, Cédric Koller<sup>b</sup>, and Lenka Zdeborová<sup>b</sup>

<sup>a</sup>Institute of Theoretical Physics, Charles University

<sup>b</sup>Statistical Physics of Computation Laboratory, École Polytechnique Fédérale de Lausanne (EPFL)

## Abstract

We investigate how much bias in the initial configuration is required to drive global agreement in synchronous, deterministic majority dynamics on large random  $d$ -regular graphs. Nodes take values  $\pm 1$  and update their states at each discrete time step to align with the majority of their neighbors. Using the backtracking dynamical cavity method (BDCM), we estimate the minimal fraction of initial  $+1$  nodes required to achieve a  $+1$  consensus in  $p$  time steps. Our analysis predicts that for  $d \geq 4$  an initial global minority of  $+1$  nodes is sufficient to quickly steer the entire system toward consensus on  $+1$ .

We then investigate whether such initial conditions can be determined explicitly for a given large random regular graph. To this end, we introduce a new algorithm, which we name *history-passing reinforcement* (HPR), designed to find such initial configurations with a minority of  $+1$  nodes. We find, as a main result, that the HPR algorithm finds initial configurations where the minority takes over the majority for  $d$ -regular random graphs with  $d \geq 4$ .

The HPR algorithm outperforms standard simulated annealing-based methods, but does not reach the lowest densities predicted by the BDCM. Rather, the lowest density achievable by the algorithm is near the onset of a dynamical one-step replica symmetry breaking (d1RSB) phase, which we estimate using a one-step replica symmetry breaking (1RSB) formulation of the BDCM. While we focus on the majority dynamics and random  $d$ -regular graphs, the algorithm can be extended to other dynamical rules and classes of sparse graphs.

## 1 Introduction

Let  $G(V, E)$  be an undirected graph with  $n$  nodes  $V = \{1, \dots, n\}$  and edges  $E = \{(i, j) \mid i, j \in V\}$ . Each node is associated with a value  $x_i \in \{-1, +1\}$ , and we define a graph configuration as  $\mathbf{x} = \{x_1, \dots, x_n\}$  with magnetization (or bias)  $m(\mathbf{x}) = \frac{1}{n} \sum_{i \in V} x_i$ . On this graph we consider the time evolution  $\mathbf{x}^t \mapsto \mathbf{x}^{t+1}$  of a synchronous local *majority dynamics* (with always-stay tie breaking): i.e. each node takes the value of the majority in their neighborhood, and in case of a tie it stays the same. Formally, for the local magnetization  $h_i^t = \sum_{j \in \partial_i} x_j^t$ , we define the update function as

$$x_i^{t+1} = f(x_i^t, \mathbf{x}_{\partial_i}^t) = \begin{cases} \text{sign}(h_i^t) & \text{if } \text{sign}(h_i^t) \neq 0, \\ x_i^t & \text{otherwise,} \end{cases} \quad (1)$$

where  $x_i^t$  denotes the state of node  $i$  at time step  $t$ ,  $\partial_i$  denotes the set of neighbors of node  $i$ , and  $\mathbf{x}_{\partial_i}^t$  contains the states of these neighbors.

This setting is motivated by a variety of spreading processes, such as the diffusion of opinions or rumors in social networks or the transmission of diseases in epidemiology. In applications, one often asks how to influence such dynamics to steer the collective outcome, i.e. which individuals to target for persuasion or the initial seeding of information or immunization, as in [38, 31, 1, 65]. From a control-and-optimization viewpoint, this is a strategic bribery problem that motivates the central question of our work on majority dynamics:

*What is the smallest initial bias that leads to a positive consensus after a fixed number of time steps?*

We consider this question for typical instances of randomly sampled graphs  $G$ , and in the large system limit  $n \rightarrow \infty$ . We define  $m_G^*(p)$  as the minimal initial bias such that for a graph  $G$  there exists an initial configuration  $\mathbf{x}^1$  with  $m(\mathbf{x}^1) = m_G^*(p)$ , and this configuration evolves to a  $+1$  consensus in  $p$  steps ( $m(\mathbf{x}^p) = 1$ ).

To this end, we study the number of initial configurations with a given bias that lead to a consensus after a fixed number of steps  $p$ , for typical instances of random  $d$ -regular graphs. We also investigate whether these initial configurations can be found on concrete graph instances using efficient algorithms.

In the following, we both establish precise estimations of the minimal biases for random  $d$ -regular graphs, and provide an algorithm that empirically finds corresponding initial configurations. While our method extends to other families of random graphs, we focus on random regular graphs (RRGs), where every node has exactly degree  $d$ :

- We analyze the problem using the backtracking dynamical cavity method (BDCM) [7], which allows for the study of short trajectories on sparse random graphs. Under the replica symmetric assumption, we find that for RRGs, for  $d \geq 4$  and  $p \geq 3$  (or  $d \geq 8$ ,  $p \geq 2$ ) there exist initializations with  $+1$  in the minority which under majority dynamics evolve into  $+1$  consensus.
- To find these initial conditions with low initial magnetization for a particular RRG, we introduce an algorithm that we name history passing reinforcement (HPR). This algorithm is based on the belief propagation reinforcement (BPR) algorithm [15, 13] which we extend to the dynamical setting. The HPR algorithm successfully finds solutions with negative  $m_{\text{init}}$  that go into positive consensus for  $d \geq 4$ . We also numerically study the performance of a simulated annealing (SA) algorithm on this problem. We find that SA does not find initializations with negative  $m_{\text{init}}$ , and that HPR outperforms it in all the considered cases. However, HPR does not reach the lowest possible bias given by the replica symmetric BDCM.
- Using the one-step replica symmetry breaking (1RSB) formulation of the BDCM, we find that replica symmetry breaks before reaching the minimal bias predicted by the replica symmetric (RS) BDCM. Nevertheless, the onset of the 1RSB phase remains in the negative-magnetization regime. Thus, BDCM still predicts the existence of strategic minorities leading to consensus. Moreover, the onset of the dynamical one-step replica symmetry breaking (d1RSB) phase roughly corresponds to the lowest algorithmically reachable  $m_{\text{init}}$ .

The code to reproduce our results, including the HPR algorithm is publicly available<sup>1</sup>. The work is structured as follows: We begin in Section 2 with an overview of related work. Section 3 introduces the BDCM formalism, both under the RS assumption and its 1RSB extension. In Section 4, we apply this framework to majority dynamics on  $d$ -regular random graphs, deriving results for the initial bias required for consensus. Section 5 then presents the HPR algorithm, designed to construct strategic initializations that drive the system to consensus. Finally, Section 6 evaluates its performance, comparing it to simulated annealing as well as to the RS and 1RSB predictions.

## 2 Related work

**Opinion dynamics** The study of opinion dynamics spans multiple disciplines, including but not limited to sociology, mathematics, physics, and computer science [18, 73, 14, 6]. Various update rules (e.g. the threshold, Galam, dissemination of culture, Sznajd, and majority models) and network topologies (e.g. fully connected, Erdős–Rényi, regular, and scale-free, sometimes dynamically changing) have been analyzed [30, 21, 22, 4, 62, 36]. We also refer the reader to [14, 66, 29] for reviews. The problem of finding an initial configuration that turns a small initial bias into a majority on one side is practically relevant in the context of bribing problems [38, 31, 1, 65, 6], and related to gerrymandering [33]. From a technical point of view, our work aligns most closely with statistical physics methods applied to opinion dynamics, a field known as sociophysics [23].

Kanoria and Montanari [36] study the majority dynamics with stochastic tie breaking on infinite regular trees and provide a lower bound on the initial number of  $+1$  opinions such that a consensus of  $+1$  is reached

---

<sup>1</sup><https://github.com/SPOC-group/history-passing>

for  $T \rightarrow \infty$ . In [26], the authors consider majority dynamics on  $d$ -RRGs, and they study how a typical small initial majority is guaranteed to reach full consensus for high  $d$ 's. However, these works only concern the average case, as the initialization is drawn uniformly at random from the possible initializations with a given density of opinions. In contrast, we aim to minimize the number of  $+1$  opinions, so an adversarial perspective is more relevant. The work [72] investigates such an adversarial approach: an attacker can choose the  $+1$  nodes, and guarantees are given when no such choice leads to a  $+1$  consensus. However, the dynamic rule of [72] is different, with the addition of “neutral” nodes taking the opinion of the majority. A broader discussion of opinion dynamics in related settings can be found in [71]. Reference [16] investigates the “Minimum Links Problem”, which seeks to achieve global consensus by adding the minimum number of new nodes and links. The work [31] studies the minimal contagious (or percolating) set problem on RRGs, which is the same optimization setting as our case, but with threshold dynamics, where nodes that reach state  $+1$  remain in it indefinitely. We also refer to this work for references to many other studies on extremal properties of graphs.

**The Mpemba effect** The problem we analyze can be interpreted as an instance of the Mpemba effect. This effect was first observed for water, where hot water can freeze faster than cold water under certain conditions [56, 35]. This phenomenon has been observed and studied in diverse settings, including spin glasses [46, 5] and colloidal systems [44]. The standard effect describes how a system starting “hotter” (further from equilibrium) may relax faster than a “colder” system. The strong version of the effect occurs when this anomalous relaxation is exponentially faster [40]. In our context, the initial magnetization  $m(\mathbf{x}^1)$  is analogous to the temperature, where initializations with lower magnetization are “hotter” with respect to the  $+1$  consensus state. Our objective of finding initial configurations with low magnetization that nevertheless reach a  $+1$  consensus is equivalent to identifying initial states that exhibit a Mpemba-like effect. These “hot” initial states follow specific efficient relaxation pathways that are inaccessible to “cold” initial states chosen at random. Therefore, the algorithm that we introduce is a tool for discovering initializations that leverage anomalous relaxation pathways.

**The cavity method** The cavity method [10, 59, 52] is a standard tool in statistical physics. The method yields a system of self-consistent equations whose solutions provide estimates of key observables. Its effectiveness has led to applications in diverse domains, for instance in theoretical computer science, e.g. for constraint satisfaction problems [54, 43, 55, 49, 60] or in the modeling of epidemic processes [37, 1, 2, 11, 27]. Its dynamical variants, usually called dynamical cavity methods or dynamical message passing, extend the method to out-of-equilibrium systems [57, 36, 3, 17, 34, 45]. Moreover, the previously introduced BDCM extends the cavity formalism to short trajectories ending in cycles [7]. The BDCM is the backbone of our analysis. By adapting the belief propagation reinforcement scheme introduced for the standard cavity method [15, 13], we obtain a solver capable of tackling problems in a dynamical setting.

### 3 The BDCM and its replica symmetry breaking extension

Our goal is to determine the smallest initial magnetization  $m_{\text{init}}$  that leads to consensus within a fixed number of time steps. To this end, we use the BDCM [7] to compute the entropy of typical initializations satisfying this criterion on large random graphs. The smallest initial bias then comes from finding the smallest  $m_{\text{init}}$  with a non-zero entropy.

In this methodological section, we first review the BDCM for general local deterministic dynamics, as originally stated in [7]. To refine the replica-symmetric (RS) estimate and capture a potentially clustered structure of satisfying configurations, we formulate it within the 1RSB framework; this has not previously been done for the BDCM. While the method is presented in general terms for deterministic dynamics on arbitrary graphs, in Section 4 we apply it specifically to majority dynamics on RRGs, to answer the question of interest.

Note that the computation for both the RS and 1RSB results are described here as approximations of the corresponding quantities on a given large random graph. This will be crucial when turning towards specific algorithms, such as the history passing reinforcement presented in Section 5. In Section 4, we then turn to

the thermodynamic limit in which, thanks to self-averaging, the single-graph results can be used to deduce the typical behavior of large random graphs.

### 3.1 Backtracking Dynamical Cavity Method

**Dynamical Processes on Graphs** For generality in this section we consider a node  $i$  to take value  $x_i \in S$  where  $S$  is a discrete set of states. Analogously, a graph configuration is  $\mathbf{x} \in S^n$ . In the following, we consider general *local*, *deterministic*, *time-discrete* and *synchronous* dynamics, where all nodes are simultaneously updated with a rule  $f_i(x_i, \mathbf{x}_{\partial i})$ . Thus, the local dynamics  $f_i : S \times S^{|\partial i|} \rightarrow S$  leads to the global dynamics  $F : S^n \rightarrow S^n$  with  $[F(\mathbf{x})]_i = f_i(x_i, \mathbf{x}_{\partial i})$ . The subsequent application of  $F$ ,  $\mathbf{x}^{t+1} = F(\mathbf{x}^t)$ , creates a *trajectory*  $\underline{x}_i = (x_i^1, \dots, x_i^T)$  at the level of each node and  $\underline{\mathbf{x}} = (\mathbf{x}^1, \dots, \mathbf{x}^T)$  at the level of the whole graph, where  $t = 1, \dots, T-1$ . Since the configuration space  $S^n$  is finite and the dynamics is deterministic, all trajectories  $\underline{\mathbf{x}}$  end in a cycle. The pre-periodic part of the trajectory is called the *transient* and the periodic part is the *attractor*. We denote the transient length as  $p$  and the attractor length as  $c$ . The set of all initializations ending in a given attractor is called its *basin of attraction*.

**The BDCM idea** A trajectory  $\underline{\mathbf{x}}$  of length  $T = p + c$ , consisting of a transient of length  $p$  followed by a cycle of length  $c$ , is called a  $(p, c)$  *backtracking attractor*. The goal of the BDCM is to count such backtracking attractors under given constraints, e.g. the number  $\mathcal{N}$  of trajectories that end in an attractor of a specific period or start with a specific magnetization. In the thermodynamic limit,  $\mathcal{N}$  generally grows exponentially with  $n$ , so we instead aim to compute the entropy density  $s = \frac{1}{n} \log(\mathcal{N})$ . The key idea, following the cavity method, is to interpret  $\mathcal{N}$  as the normalization constant of a uniform measure supported only on admissible backtracking attractors. Although the underlying object of interest, the backtracking attractor, captures dynamical properties, we approach it through a static formulation. By encoding admissible trajectories into a probability measure, the counting problem reduces to evaluating the normalization constant. Within the RS ansatz, this normalization can be estimated from a set of fixed-point equations, giving access to an estimate of the typical count in the thermodynamic limit. The RS ansatz thus provides the natural starting point for the analysis, but it is limited: the resulting estimate gives only an upper bound on the asymptotical entropy [19], and when the space of solutions has a clustered structure it may not be accurate. We address the latter case via 1RSB, which is presented in Section 3.2. We can also refine the constraints on the backtracking attractors by reweighting the probability measure, biasing it toward trajectories with the desired properties.

**A probability measure over backtracking attractors** More formally, we can define the following measure on backtracking attractors  $\underline{\mathbf{x}} \in S^{p+c}$ , where  $\underline{\mathbf{x}}$  is a valid trajectory of length  $p$  that ends in a cycle of length  $c$  and we reweight every  $\underline{\mathbf{x}}$  according to  $K$  observables  $\Xi_k$ :

$$P(\underline{\mathbf{x}}) = \frac{1}{Z} e^{-\sum_k \lambda_k \Xi_k(\underline{\mathbf{x}})} \mathbb{1}[\underline{\mathbf{x}}^{p+1} = F(\underline{\mathbf{x}}^{p+c})] \prod_{t=1}^{p+c-1} \mathbb{1}[\underline{\mathbf{x}}^{t+1} = F(\underline{\mathbf{x}}^t)]. \quad (2)$$

$Z$  is the normalization constant of the probability distribution, and  $\mathbb{1}[s]$  is the indicator function<sup>2</sup>.

The set  $\{\Xi_k\}_{k=1}^K$  contains functions that represent extensive observables<sup>3</sup> on these backtracking attractors, with  $\Xi : S^{n(p+c)} \rightarrow \mathbb{R}$ . They can represent properties such as the initial magnetization or the number of times a node changes value throughout the trajectory. We denote their intensive counterparts  $\{\Xi_k(\underline{\mathbf{x}})/n\}_{k=1}^K$  as  $\{\xi_k\}_{k=1}^K$ .

**Computing the entropy density** The BDCM's objective is to express the number of valid backtracking attractors conditioned on the observable values  $\{\xi_k\}_{k=1}^K$ ,  $\mathcal{N}(\{\xi_k\}_{k=1}^K)$ , via the *entropy density*:

$$s(\{\xi_k\}_{k=1}^K) = \frac{\log \mathcal{N}(\{\xi_k\}_{k=1}^K)}{n}. \quad (3)$$

<sup>2</sup> $\mathbb{1}[s]$  is 1 if the boolean statement  $s$  is true and 0 otherwise.

<sup>3</sup> $\Xi(\underline{\mathbf{x}}) \sim O(n)$  as  $n \rightarrow \infty$

The entropy  $s(\{\xi_k\}_{k=1}^K)$  is related to the normalization constant  $Z$  through the following transformation:

$$\begin{aligned} Z &= \sum_{\{\underline{\mathbf{x}}\}} e^{-\sum_k \lambda_k \Xi_k(\underline{\mathbf{x}})} \mathbb{1} [\mathbf{x}^{p+1} = F(\mathbf{x}^{p+c})] \prod_{t=1}^{p+c-1} \mathbb{1} [\mathbf{x}^{t+1} = F(\mathbf{x}^t)] \\ &= \sum_{\{\xi_k\}_{k=1}^K} \mathcal{N}(\{\xi_k\}_{k=1}^K) e^{-\sum_k \lambda_k \Xi_k(\underline{\mathbf{x}})} \simeq \int \left( \prod_{k=1}^K d\xi_k \right) e^{n[s(\{\xi_k\}_{k=1}^K) - \sum_{k=1}^K \lambda_k \xi_k]} , \end{aligned} \quad (4)$$

where the last expression is valid in the large  $n$  limit, in which the intensive quantities take the same values for almost every realization of the graph, the so-called self-averaging of statistical physics of disordered systems [53]. Defining the *free entropy density* as  $\Phi(\{\lambda_k\}_{k=1}^K) = \log Z/n$  and applying the saddle point method, this connects the entropy density to  $Z$  in the large  $n$  limit as

$$s(\{\hat{\xi}_k\}_{k=1}^K) = \Phi(\{\lambda_k\}_{k=1}^K) + \sum_k \lambda_k \hat{\xi}_k , \quad (5)$$

where we denote as  $\{\hat{\xi}\}_{k=1}^K$  the maximizer of  $s(\{\xi_k\}_{k=1}^K) - \sum_k \lambda_k \xi_k$ . Thus, we have the following conditions for all  $k = 1, \dots, K$ :

$$\frac{\partial \Phi(\lambda_1, \dots, \lambda_K)}{\partial \lambda_k} = -\hat{\xi}_k = -\frac{1}{n} \langle \Xi_k \rangle_{P(\underline{\mathbf{x}})} . \quad (6)$$

Consequently, if we know  $\Phi(\{\lambda_k\}_{k=1}^K)$  for an arbitrary set of Lagrange parameters  $\{\lambda_k\}_{k=1}^K$ , we can also obtain the entropy density  $s(\{\xi_k\}_{k=1}^K)$  with fixed observables  $\{\xi_k\}_{k=1}^K$  from (5). These observables are enforced by values of  $\{\lambda_k\}_{k=1}^K$ , as seen in (6).

**Estimating the normalization constant via Belief Propagation** Computing  $\Phi$  or  $Z$  on a given graph exactly is intractable in general, as we have an exponential number of trajectories  $\underline{\mathbf{x}}$ . However, on large random graphs, we can estimate  $\Phi$  using the cavity method [49, 42]. For this, we represent the probability distribution (2) as a tree-like graphical model. By definition, the dynamics  $F(\mathbf{x})$  factorizes on the node neighborhoods. We similarly assume that the global observables  $\Xi$  can be factorized over the nodes  $V$  via  $\Xi(\underline{\mathbf{x}}) = 1/n \sum_{i \in V} \tilde{\Xi}(x_i)$  or analogously over the edges  $E$ <sup>4</sup>. Then, we can factorize the whole probability distribution (2) as

$$P(\underline{\mathbf{x}}) = \frac{1}{Z} \prod_{i \in V} \underbrace{\left[ e^{-\sum_{\bar{k}} \lambda_{\bar{k}} \tilde{\Xi}_{\bar{k}}(x_i)} \mathbb{1} [x_i^{p+1} = f_i(x_i^{p+c}, \mathbf{x}_{\partial i}^{p+c})] \prod_{t=1}^{p+c-1} \mathbb{1} [x_i^{t+1} = f_i(x_i^t, \mathbf{x}_{\partial i}^t)] \right]}_{\mathcal{A}_i(\underline{x}_i, \underline{\mathbf{x}}_{\partial i})} \prod_{(ij) \in E} \underbrace{\left[ e^{-\sum_{\bar{k}} \lambda_{\bar{k}} \tilde{\Xi}_{\bar{k}}(\underline{x}_i, \underline{x}_j)} \right]}_{a(\underline{x}_i, \underline{x}_j)} , \quad (7)$$

where we define the factor nodes  $\mathcal{A}_i(\underline{x}_i, \underline{\mathbf{x}}_{\partial i})$  and  $a(\underline{x}_i, \underline{x}_j)$ . When we can interpret this distribution as a tree factor graph (described in detail in Appendix A), we can use belief propagation to compute  $Z$ . We do this by introducing *messages*  $\chi_{\underline{x}_i, \underline{x}_j}^{i \rightarrow j} \in \mathbb{R}$ . The messages correspond to the probability of node trajectories  $\underline{x}_i, \underline{x}_j$  taking on specific values when we restrict ourselves to a particular subpart of the factor graph (on the original graph  $G$  this corresponds to focusing on a subgraph containing node  $i$  after omitting the edge  $(ij)$ , i.e. after introducing cavity). For these messages we arrive at the following equations (see Appendix A for details)

$$\chi_{\underline{x}_i, \underline{x}_j}^{i \rightarrow j} = \frac{1}{Z^{i \rightarrow j}} a(\underline{x}_i, \underline{x}_j) \sum_{\underline{\mathbf{x}}_{\partial i \setminus j}} \mathcal{A}_i(\underline{x}_i, \underline{\mathbf{x}}_{\partial i}) \prod_{k \in \partial i \setminus j} \chi_{\underline{x}_k, \underline{x}_i}^{k \rightarrow i} . \quad (8)$$

<sup>4</sup>We denote by  $\tilde{\Xi}(x_i) : S^{p+c} \rightarrow \mathbb{R}$  observables depending on single nodes and by  $\tilde{\Xi}(\underline{x}_i, \underline{x}_j) : S^{2(p+c)} \rightarrow \mathbb{R}$  observables depending on two nodes connected by an edge.

Messages that fulfill this recurrence can be used to obtain an estimate of  $\Phi$  called the *Bethe free entropy density*  $\Phi_B$ :

$$n\Phi_B = \sum_{i \in V} \log(Z^i) - \sum_{(ij) \in E} \log(Z^{ij}), \quad (9)$$

$$Z^i = \sum_{\underline{x}_i, \underline{x}_{\partial i}} \mathcal{A}_i(\underline{x}_i, \underline{x}_{\partial i}) \prod_{j \in \partial i} \chi_{\underline{x}_j, \underline{x}_i}^{j \rightarrow i}, \quad (10)$$

$$Z^{ij} = \sum_{\underline{x}_i, \underline{x}_j} \frac{1}{a(\underline{x}_i, \underline{x}_j)} \chi_{\underline{x}_i, \underline{x}_j}^{i \rightarrow j} \chi_{\underline{x}_j, \underline{x}_i}^{j \rightarrow i}. \quad (11)$$

The derivation of these relations can also be found in Appendix A. The Bethe free entropy density calculated by (9) from the converged BDCM messages gives the asymptotically exact value of the free entropy density in the thermodynamic limit (again relying on self-averaging) even for *non-tree* graphs if the RS assumption holds. This assumption translates into the independence of the incoming messages to any factor node. We describe how to approach the case where the RS assumption breaks down in the following and in Appendices A and B.

### 3.2 Replica Symmetry Breaking for BDCM

This section summarizes the one-step replica symmetry breaking version of the BDCM; detailed derivations are deferred to Appendix B. The concept of replica symmetry breaking was introduced by Parisi [58] via the replica method and later formulated within the cavity method [50, 51], the approach we adopt here. A comprehensive treatment of the cavity formalism for RSB can be found in [49].

The assumption behind 1RSB is that the space of solutions splits into multiple distinct clusters, and each cluster is associated with a fixed point of the BDCM equations. Let  $P_{1\text{RSB}}(\tilde{\chi})$  be the following Boltzmann distribution over the fixed points  $\tilde{\chi} = \{\chi^{i \rightarrow j}, \chi^{j \rightarrow i}\}_{(ij) \in E}$  with  $\chi^{i \rightarrow j} = \{\chi_{\underline{x}_i, \underline{x}_j}^{i \rightarrow j}\}_{(\underline{x}_i, \underline{x}_j) \in S^{2(p+c)}}$ :

$$P_{1\text{RSB}}(\tilde{\chi}) = \frac{1}{Z_{1\text{RSB}}(r)} e^{nr\Phi_{\text{int}}(\tilde{\chi})}. \quad (12)$$

Here,  $r$  is the *Parisi parameter*.  $Z_{1\text{RSB}}$  is the normalization and  $\Phi_{\text{int}}(\tilde{\chi})$  the Bethe free entropy density computed from the fixed point  $\tilde{\chi}$  according to equation (9). We call it the *internal free entropy density* as it is the free entropy density of a cluster. We define the *replicated free entropy density* as

$$\Psi(r) = \frac{\log Z_{1\text{RSB}}(r)}{n}. \quad (13)$$

Furthermore, the entropy density of clusters with internal free entropy density  $\Phi_{\text{int}}$  is given by the *complexity*  $\Sigma(\Phi_{\text{int}})$

$$\Sigma(\Phi_{\text{int}}) = \frac{\log \mathcal{N}(\Phi_{\text{int}})}{n}, \quad (14)$$

where  $\mathcal{N}(\Phi_{\text{int}})$  is the total number of clusters with internal free entropy density  $\Phi_{\text{int}}$ .

Expressing  $Z_{1\text{RSB}}$  as an integral over the internal free entropies and applying the saddle-point method, we obtain in the thermodynamic limit

$$\Psi(r) = r\hat{\Phi}_{\text{int}} + \Sigma(\hat{\Phi}_{\text{int}}), \quad (15)$$

where  $\hat{\Phi}_{\text{int}}$  extremizes  $\Psi(r)$ . The *total free entropy density* is defined as

$$\Psi_{\text{tot}} = \Phi_{\text{int}} + \Sigma(\Phi_{\text{int}}), \quad (16)$$

where  $\Phi_{\text{int}}$  maximizes  $\Psi_{\text{tot}}$  under the constraint  $\Sigma(\Phi_{\text{int}}) \geq 0$  (there must exist at least one cluster). Intuitively, *typical solutions* are those that jointly maximize  $\Phi_{\text{int}}$  (the size of the clusters) and  $\Sigma$  (the number of clusters). Ignoring the constraint  $\Sigma(\Phi_{\text{int}}) \geq 0$ , the total free entropy density is maximized for  $r = 1$  by  $\hat{\Phi}_{\text{int}}$ .

If the complexity for  $r = 1$  is positive, the problem is in the d1RSB phase. The problem admits exponentially many thermodynamically relevant clusters with internal free entropy density  $\Phi_{\text{int}} = \hat{\Phi}_{\text{int}}$ .

When the complexity is negative for  $r = 1$ ,  $r$  must be changed until  $\Sigma \geq 0$  to obtain a physically meaningful result. The total entropy is then maximized for  $r < 1$  such that  $\Sigma = 0$  (see Appendices B.2 and B.4 for additional details) the problem is said to be in the static one-step replica symmetry breaking (s1RSB) phase. The problem admits a sub-exponential number of thermodynamically relevant clusters ( $\Sigma = 0$ ).

The RS and d1RSB BDCM estimates of the total entropy density (9) are equivalent. In the presence of s1RSB, the RS and s1RSB entropy are not equivalent, the later is smaller, and both provide an upper estimate of the exact asymptotic entropy density [19]. Note that additional steps of replica symmetry breaking are possible, but we do not check for them.

Computing the observables in the 1RSB setting is again done using the cavity method. This is described in Appendix B.2 together with the population dynamics algorithm (Appendix B.3) used to approximate the solution of the 1RSB BDCM equations, which are now over probability distributions.

## 4 Results for Minority Takeover on Random Regular Graphs

We return to our initial question: “*For majority dynamics, what is the smallest initial bias that leads to consensus after a fixed number of time steps?*” To build some intuition for this specific dynamical system on regular graphs, it is useful to recall some of its general properties. In particular, majority dynamics admits attractors of exactly two lengths,  $c \in \{1, 2\}$  [28], and there are four dominant attractor types [7]: the two  $\pm 1$  consensus states; a stable period-1 state with a finite fraction of both spins; and a period-2 state where some nodes flip repeatedly. The typical behavior of initial configurations with a fixed initial magnetization on a 4-regular random graph illustrates the general phenomenology. Initializations with  $m_{\text{init}} \lesssim -0.5$  converge<sup>5</sup> to a value of  $-1$  in the attractor, and  $m_{\text{init}} \gtrsim 0.5$  converge to  $+1$ . Figure 1 (left) shows the RS estimation of the entropy as function of the initial magnetization. The transition between the mixed state and  $+1$  consensus empirically lies at  $m_{\text{sample}}^*(\infty) \sim 0.46$ . This marks the point where upon random sampling of a configuration with  $m_{\text{init}} > m_{\text{sample}}^*$  and a large enough time budget  $p$ , the nodes will eventually reach  $+1$  consensus [7].

However, these results do not tell us whether initializations that reach  $+1$  consensus and have the magnetization smaller than  $m_{\text{sample}}^*$  exist, whether they converge quickly, and whether they can be found algorithmically. In this section, we apply the formalism introduced in the previous section to estimate the minimal initial magnetization within the RS assumption, and we study when this assumption breaks down with the 1RSB formalism.

### 4.1 BDCM Equations for Majority Dynamics on Random Regular Graphs

To investigate the above questions, we will use the BDCM to compute the smallest magnetization for which the replica symmetric entropy is non-negative, denoting

$$m_{\text{RS}}^*(d, p) = \arg \min_m s_{\text{RS}}(m; d, p) \geq 0, \quad (17)$$

where  $s_{\text{RS}}(m; d, p)$  denotes the replica-symmetric entropy of backtracking attractors that reach  $+1$  within fixed  $p$  steps. Since the RS entropy is an upper bound on the true asymptotic entropy, minimizing over  $m_{\text{init}}$  gives the lower bound on  $m^*(p)$ .

The BDCM probability distribution (7) for the majority dynamics simplifies to

$$P(\underline{x}) = \frac{1}{Z} \prod_{i \in V} \underbrace{\left[ e^{-\lambda_{\text{init}} x_i^1} \mathbb{1} [x_i^{p+1} = +1] \prod_{t=1}^p \mathbb{1} [x_i^{t+1} = f_i(x_i^t, \mathbf{x}_{\partial i}^t)] \right]}_{\mathcal{A}(x_i, \mathbf{x}_{\partial i})}, \quad (18)$$

where  $\lambda_{\text{init}}$  is the Lagrange parameter associated with the initial magnetization  $m_{\text{init}}(\mathbf{x}) = \frac{1}{n} \sum_i x_i^1$ .

To simplify the equation further, we use the symmetry of RRGs. In the thermodynamic limit, the neighborhood around each node becomes identical, and hence the fixed points of the BDCM equations

<sup>5</sup>After possibly  $p = 2^n$  steps.

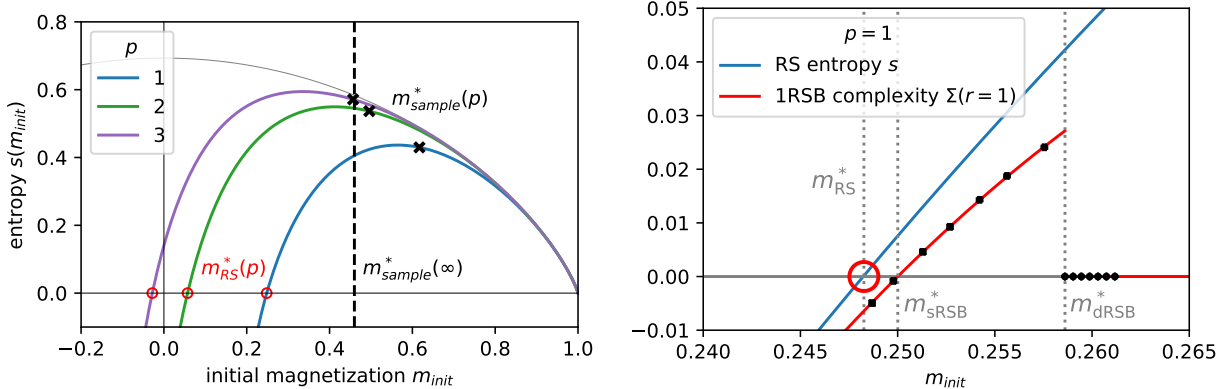


Figure 1: **Always-stay majority dynamics on 4-regular random graphs.** (Left) Replica symmetric entropy on initializations going to a positive consensus in  $p$  steps as a function of the initial magnetization obtained from BDCM for  $d = 4$  and  $p = 1, 2, 3$ . We mark the replica symmetric lower bound  $m_{RS}^*(p)$ , and the magnetization  $m_{sample}^*(p)$  as the one at which +1 consensus becomes the entropically dominating attractor [7]. The gray line represents the total entropy of all configurations. (right) Zoom into the region where the entropy becomes negative for the  $p = 1$  case. The red line shows the complexity (eq. 14) at Parisi parameter  $r = 1$ . The dashed grey lines denote the initial magnetizations at which the d1RSB and s1RSB phases emerge, as well as the point where the RS entropy crosses 0.

$\chi_{\underline{x}_i, \underline{x}_j}^{i \rightarrow j}$  (8) are the same for all  $i, j$  [67]. Consequently, we can consider one edge-independent set of message values  $\chi_{\underline{x}, \underline{y}}^{\rightarrow}$ , and find fixed points for all trajectory combinations  $(\underline{x}, \underline{y}) \in \{\pm 1\}^{2(p+1)}$  of the following equation

$$\chi_{\underline{x}, \underline{y}}^{\rightarrow} = \frac{1}{Z^{\rightarrow}} \sum_{\underline{y}_{[d-1]}} \mathcal{A}(\underline{x}, \underline{y}_{[d]}) \prod_{\underline{y} \in \underline{y}_{[d-1]}} \chi_{\underline{y}, \underline{x}}^{\rightarrow}, \quad (19)$$

where  $\underline{y}_{[d-1]}$  are the trajectories  $(\underline{y}_1, \dots, \underline{y}_{d-1})$  of the  $d-1$  neighboring messages, and  $Z^{\rightarrow}$  is the normalization as before. From the converged message values  $\chi_{\underline{x}, \underline{y}}^{\rightarrow}$ , we compute the Bethe free entropy density as

$$\Phi_B = \log(Z^{\text{fac}}) - \frac{d}{2} \log(Z^{\text{var}}), \quad (20)$$

$$Z^{\text{fac}} = \sum_{\underline{x}, \underline{y}_{[d]}} \mathcal{A}(\underline{x}, \underline{y}_{[d]}) \prod_{\underline{y} \in \underline{y}_{[d]}} \chi_{\underline{y}, \underline{x}}^{\rightarrow}, \quad (21)$$

$$Z^{\text{var}} = \sum_{\underline{x}, \underline{y}} \chi_{\underline{x}, \underline{y}}^{\rightarrow} \chi_{\underline{y}, \underline{x}}^{\rightarrow}. \quad (22)$$

Note that the obtained quantities are now averages over the ensemble of RRGs that thanks to self-averaging capture the behavior of typical large random graphs (modulo the RS assumption). Using  $\Phi_B$ , we can again compute the entropy density  $s(m_{init})$  using equations (5) and (6). This quantity provides the exponentially leading number of valid  $(p+1)$  backtracking attractors with  $m_{\text{attr}} = 1$ , conditioned on a fixed value of  $m_{init}$ . Knowing the function  $s(m_{init})$  allows us to analyze the system's behavior when initialized with a given  $m_{init}$ . In particular,  $m_{init}$  such that  $s(m_{init}) = 0$  is the minimal initial magnetization of trajectories that reach full consensus in  $p$  steps, i.e. it is the  $m_{RS}^*(d, p)$  from (17).

## 4.2 Replica Symmetric Results

The analysis of [7] shows that running the dynamics until convergence from a random initialization with  $m_{init} > m_{sample}^*(d)$  will typically reach +1 consensus. For a fixed  $p$ ,  $m_{sample}^*(p, d)$  describes the smallest value for which a randomly sampled backtracking attractor of fixed path length  $p$  typically reaches +1 consensus<sup>6</sup>.

<sup>6</sup>Under the replica symmetric assumption, but this was checked to be correct for these values of  $m_{init}$  in [7]

It can be obtained by comparing the entropy of the backtracking attractors with the four other possible attractors and then determine which one is entropically dominant. This is shown as the dashed line for large  $p$  and crosses for  $p = 1, 2, 3$  in Figure 1 (left), and also in Table 2.

However, while  $m_{\text{sample}}^*(p, d)$  characterizes typical initializations when +1 consensus dominates entropically, we are interested in exploring the more extreme cases: initial configurations that start farthest from the majority yet still reach full +1 consensus. Accordingly, we restrict our analysis to backtracking attractors that lead to consensus and consider the smallest  $m_{\text{init}}$  under the replica-symmetric assumption, called  $m_{\text{RS}}^*(d, p)$ , for which their entropy is non-negative (17). The entropy of these backtracking attractors is shown in Figure 1 (left) as a function of the initial magnetization for  $d = 4$ . We mark the points  $m_{\text{RS}}^*(p)$  where the entropy becomes negative. This approach predicts the existence of initializations in 4-RRGs with negative magnetization (up to  $-0.0281(1)$ ) that evolve into the all-ones attractor within  $p = 3$  steps under majority dynamics.

$d$	$p$					
	1	2	3	4	5	6
3	0.369	0.188	0.106	0.065	0.046	0.033
4	0.248	0.057	<b>-0.028</b>	<b>-0.076</b>		
5	0.261	0.057	<b>-0.040</b>			
6	0.206	0.010	<b>-0.079</b>			
7	0.213	0.009	<b>-0.086</b>			
8	0.179	<b>-0.015</b>	<b>-0.100</b>			
9	0.184	<b>-0.016</b>	<b>-0.106</b>			
10	0.161	<b>-0.029</b>				
11	0.164	<b>-0.031</b>				
12	0.147	<b>-0.038</b>				

Table 1: Values for  $m_{\text{RS}}^*(d, p)$ , the RS minimal initial magnetization leading to consensus in  $p$  steps for majority dynamics and always-stay tie breaking on  $d$ -RRGs. It is given by the last  $m_{\text{init}}$  for which the RS BDCM calculation returns a non-negative entropy density. We highlight the negative values of  $m_{\text{init}}$ , which indicate that there might exist initializations with a *minority* of +1 opinions that still lead to a full +1 consensus.

This is not only much lower than the randomly sampled initializations  $m_{\text{sample}}^*$ , but shows that there exist initializations with a minority of +1's where they become the majority through majority dynamics. While it is perhaps unsurprising that such initializations should exist for regular but adversarially chosen graphs with carefully designed structure, this result indicates that such initializations exist for typical randomly sampled graphs.

This phenomenon is not restricted to 4-regular graphs. In Table 1 we show the minimal initial magnetization that achieves zero entropy for different combinations of degrees  $d$  and trajectory lengths  $p$ . We highlight the lower bounds  $m_{\text{RS}}^*$  that are negative in bold, as only in those cases minority-initialized configurations can potentially achieve full consensus. This is the case for all  $d \geq 8$  with trajectory lengths  $p = 2$  or for  $d \geq 4$  with  $p = 3$ . For  $p = 1$  finding such typical initializations for a smaller than zero bias seems infeasible.

In Figure 2 (left) we extrapolate the finite  $d$  results up until  $d \leq 249$ . Even degree settings for lower  $d$ s show lower minimal  $m_{\text{init}}$ . This stems from the tie breaking applied in even degrees. The initial magnetization follows a scaling as  $m_{\text{RS}}^*(d) \sim 1/\sqrt{d}$ , eventually reaching zero for  $d = \infty$ . This indicates that for  $p = 1$   $m_{\text{init}} < 0$  is not reached. This is consistent with the result expected for a fully connected graph with  $d = n - 1$ : More than half of the nodes need to be in state +1 to arrive at consensus in a single step, hence we must have  $m_{\text{init}} > 0$  if we want to arrive there in a single step.

For the case  $d = 3$  we were not able to directly find a  $p$  which admits a negative  $m_{\text{RS}}^*(p)$ . An extrapolation scaling as  $1/p \rightarrow 0$ , Figure 2 (right), indicates that our results would be compatible with the case  $m_{\text{RS}}^*(p) < 0$  for  $p \geq 13$ . However, given the scarcity of data points, this extrapolation should be treated with particular caution. We leave the problem of finding initializations for which minority takes over majority for 3-random regular graphs as an open question.

Importantly, the results in this section are only asymptotically exact under the replica-symmetric assumption.

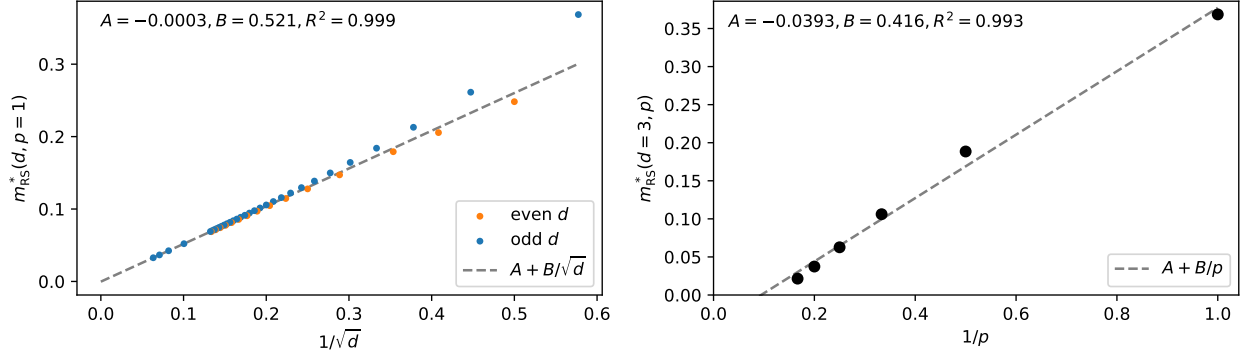


Figure 2: Extrapolation of the RS minimal initial magnetization leading to +1 consensus under majority dynamics with always-stay tie breaking on  $d$ -RRGs. (Left)  $m_{\text{RS}}^*(d)$  for  $p = 1$  as a function of  $1/\sqrt{d}$ . The linear fit for points with  $d \geq 40$  ( $1/\sqrt{d} \leq 0.158$ ) is shown. (Right)  $m_{\text{RS}}^*(p)$  for  $d = 3$  as a function of  $1/p$ . All points are used in the fit.

tion. In [7], stability checks of the RS equations were performed only for the entropically dominant solutions with  $m_{\text{init}} > m_{\text{sample}}^*(p, d)$ . There, the results indicated that the RS assumption held true. However, as the initial magnetization  $m_{\text{init}}$  decreases, the constraints on the system become increasingly difficult to satisfy, as evidenced by the decreasing entropy shown in Figure 1. Consequently, it is natural to expect the solution space to become increasingly clustered at low  $m_{\text{init}}$  values, indicating that the 1RSB assumption may be required.

### 4.3 Replica Symmetry Breaking for Small Initial Magnetizations

We recall that Section 3.2 introduces the replica symmetry breaking formalism and that Appendix B.2 presents the derivation of the 1RSB BDCM equations. Using the population dynamics procedure described in Appendix B.3, we find a numerical solution to these equations and identify the value of  $\lambda_{\text{init}}$  at which the d1RSB transition occurs and then compute the corresponding initial magnetization  $m_{\text{dRSB}}^*$ . Similarly, we find the initial magnetization  $m_{\text{sRSB}}^*$ . These values are noted in Table 2.

The structural changes of the solution space associated with the 1RSB are captured by the complexity  $\Sigma$ , defined in (14). The complexity  $\Sigma$  becomes strictly positive at  $m_{\text{dRSB}}^*$  when the problem enters the d1RSB phase, as exponentially many clusters appear. In this phase, the geometry of the solution space changes, but the observables of the problem (entropy, magnetization, etc.) remain the same as in the RS phase. The RS observables of the problem cease to be asymptotically exact in the s1RSB phase, when the complexity at  $r = 1$  becomes negative. This is illustrated in Figure 1 (right) in the case  $p = 1, d = 4$ . The figure shows the RS entropy and the complexity (14) with Parisi parameter  $r = 1$  as a function of  $m_{\text{init}}$ . Figure 3 shows the entropy and complexity curves for other degrees and  $p = 1$ , while higher  $p$ s are shown in Appendix B.4.

Another question of interest that can be answered by the 1RSB analysis is whether the solutions are *frozen*. A node trajectory from a given solution is said to be frozen if it takes the same value for all solutions within its cluster. If a cluster contains an extensive number of frozen trajectories, it is said to be *frozen*. The emergence of an extensive number of frozen trajectories in *typical* solutions marks the *rigidity transition*, and this phase is called rigid. The transition at which *all* clusters (including atypical ones) become frozen is known as the *freezing transition*, and the corresponding phase is referred to as frozen [20].

We can estimate the fraction of frozen trajectories from the approximate solution obtained from the population dynamics. This is done by counting the number of messages in the population that imply a fixed trajectory value, that is, messages that are “delta peaked” at a specific trajectory. Our numerical results show that, as soon as the d1RSB phase is entered, a finite fraction of the messages are almost peaked, in that they assign a probability close to 1 to a specific trajectory. The obtained probability distributions are shown in Figure 10 in Appendix B.5. However, this probability is not exactly 1, which we attribute to numerical approximations. Alternatively, it is also possible that the messages are in fact only “almost peaked” (these are called *quasi-hard fields* in [68]). In this case, distinguishing freezing and quasi-freezing is hard to

p		d			
		3	4	5	6
1	$m_{\text{sample}}^*$	0.777	0.617	0.443	0.398
	$m_{\text{dRSB}}^*$	0.379	0.258	0.274	0.221
	$m_{\text{sRSB}}^*$	0.376	0.250	0.263	0.206
	$m_{\text{RS}}^*$	0.369	0.247	0.261	0.206
2	$m_{\text{sample}}^*$	0.692	0.496	0.302	0.255
	$m_{\text{dRSB}}^*$	0.199*	0.075*	0.081*	0.039*
	$m_{\text{sRSB}}^*$	0.191	0.064	0.063	0.015
	$m_{\text{RS}}^*$	0.188	0.056	0.057	0.010
3	$m_{\text{sample}}^*$	0.643	0.457	0.231	0.188
	$m_{\text{dRSB}}^*$	0.117*	-0.005*	-	-
	$m_{\text{RS}}^*$	0.106	-0.028	-0.039	-0.079

Table 2: Thresholds of the initial magnetization where typical initializations cease to go to +1 consensus ( $m_{\text{sample}}^*$ ), where d1RSB appears ( $m_{\text{dRSB}}^*$ ), where s1RSB appears ( $m_{\text{sRSB}}^*$ ) and where the RS entropy crosses zero ( $m_{\text{RS}}^*$ ). The values  $m_{\text{sample}}^*$  for  $d = 3, 4, 5$  are from [8], while the case  $d = 6$  is discussed in Appendix A.1. The values with an asterisk are an upper bound on the d1RSB phase, stemming from the last RS stable values of  $m_{\text{init}}$ . For  $p = 3$  and  $d = 5, 6$ , numerical instabilities in the population dynamics procedure rendered the identification of the d1RSB phase inconclusive. Similarly, the s1RSB threshold is not noted for  $p = 3$  (see Appendix B.4).

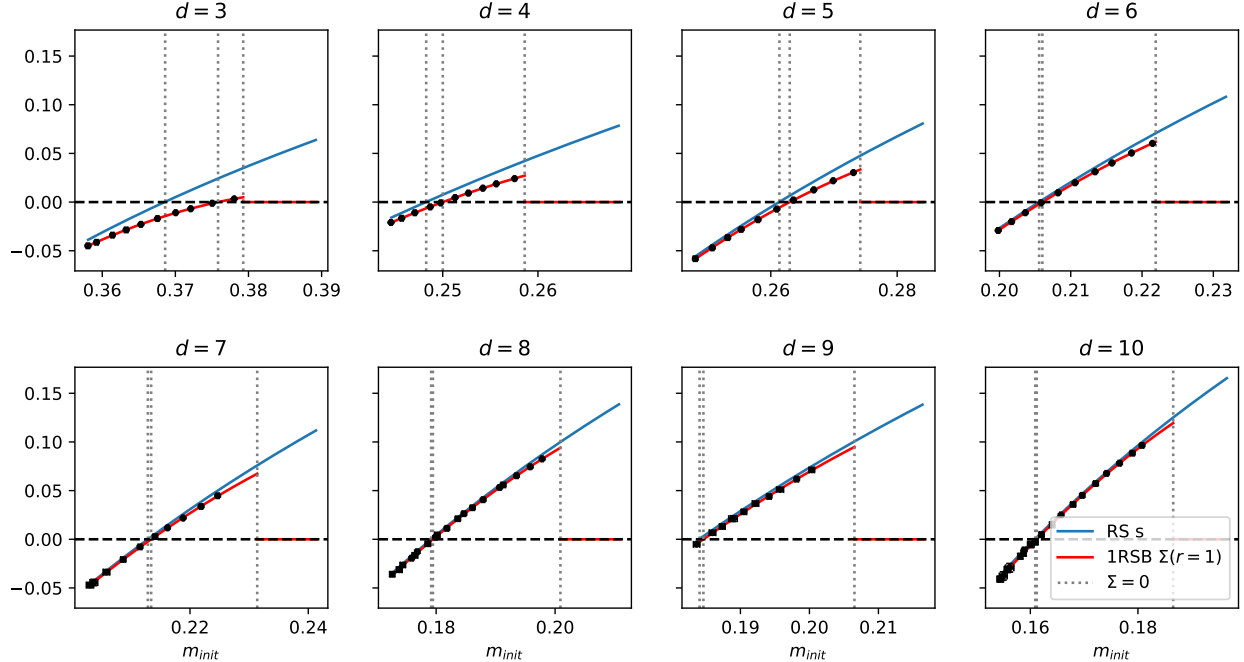


Figure 3: Thresholds of  $m_{\text{RS}}^*$ ,  $m_{\text{sRSB}}^*$  and  $m_{\text{dRSB}}^*$  (vertical lines from left to right) for  $p = 1$  and different values of  $d$ . Each black point represents the complexity  $\Sigma$  obtained from the 1RSB equations for a single  $\lambda$ , and the error on the sample mean is indicated by error bars in  $x$  and  $y$  over 10 samples. The red curve is a quadratic fit of this data, which ends at  $m_{\text{dRSB}}^*$  from Table 2.

do numerically. Nonetheless, we favor the hypothesis of true freezing, as the threshold closely matches the performance of the HPR algorithm, as will be discussed below. Moreover, Figure 3 shows that for larger

values of  $d$ , the complexity approaches the entropy. This indicates that the solution space becomes highly clustered, with only a small number of solutions contained within each cluster. Although this phenomenon is not necessary for freezing, it is typical as few solutions within each cluster are often related to many frozen variables. Numerical experiments and further discussion on the freezing can be found in Appendix B.5.

## 5 History Passing Reinforcement

We are inspired by the well-known breakthrough of the survey propagation algorithm [54] that turned a cavity method solution into an algorithm that was able to solve unprecedentedly hard and large random satisfiability instances. Here we use the same idea for the replica symmetric version of the analysis method. The HPR algorithm is a *dynamical* variation of the belief propagation reinforcement procedure [15, 13] that utilizes the BDCM described in Section 3. For a particular  $d$ -RRG, we want to find its initialization that leads to a +1 consensus in  $p$  steps, but starts with +1 nodes in minority. We refer to such an initialization as a *solution*.

The BDCM messages  $\chi_{\underline{x}_i, \underline{x}_j}^{i \rightarrow j}$  provide estimates of marginal probabilities for node trajectories. Thus, running the BDCM equations on a given graph offers guidance on the structure of promising initializations. The HPR algorithm exploits these marginals by reinforcing messages corresponding to higher-probability trajectory values, while suppressing those with lower probability. For example, if a node is likely to start in state  $-1$ , this information is propagated to its neighbors through reinforced updates. Iterative reinforcement in this way sharpens the marginals to better satisfy the constraints, gradually biasing them toward the desired initial node values.

Concretely, this leads to the addition of biases  $b_{x_i}^i$  to every message  $\chi_{\underline{x}_i, \underline{x}_j}^{i \rightarrow j}$  in the BDCM fixed-point equation:

$$\chi_{\underline{x}_i, \underline{x}_j}^{i \rightarrow j} = \frac{1}{Z^{i \rightarrow j}} \sum_{\underline{x}_{\partial i \setminus j}} \mathcal{A}_i(\underline{x}_i, \underline{x}_{\partial i}) \prod_{k \in \partial i \setminus j} b_{x_k}^k \chi_{\underline{x}_k, \underline{x}_i}^{k \rightarrow i}. \quad (23)$$

We consider binary states, so we have two scalar bias values  $b_1^i$  and  $b_{-1}^i$  for each message. The following heuristic is used to update the bias values:

$$\begin{aligned} b_1^i &= \pi, & b_{-1}^i &= 1 - \pi, & \text{if } \mu_{x_i^1=1}^i < \mu_{x_i^1=-1}^i, \\ b_1^i &= 1 - \pi, & b_{-1}^i &= \pi, & \text{if } \mu_{x_i^1=1}^i \geq \mu_{x_i^1=-1}^i, \end{aligned} \quad (24)$$

where  $\pi \in [0, 1/2]$  is a hyperparameter. The marginal  $\mu_{x_i^1=s}^i$ , with  $s \in \{\pm 1\}$  is the BDCM estimate on the marginal probability that  $x_i^1 = s$  for the variable node  $(\underline{x}_i, \underline{x}_j)$ . Note that setting  $\pi = 1/2$  results in the unmodified BDCM equations due to normalization, and lowering  $\pi$  leads to stronger reinforcement. The marginals are computed as

$$\mu_{x_i^1=s}^i = \frac{1}{Z_\mu} \prod_{j \in \partial i} Z_{x_i^1=s}^{ij}, \quad (25)$$

where  $Z_\mu$  is the normalization of the marginals:  $Z_\mu = \sum_{s \in \{\pm 1\}} \prod_{j \in \partial i} Z_{x_i^1=s}^{ij}$ , and  $Z_{x_i^1=s}^{ij}$  is defined as

$$Z_{x_i^1=s}^{ij} = \frac{1}{Z_c} \sum_{\underline{x}_i, \underline{x}_j} \mathbb{1} [x_i^1 = s] \chi_{\underline{x}_i, \underline{x}_j}^{i \rightarrow j} \chi_{\underline{x}_j, \underline{x}_i}^{j \rightarrow i}, \quad (26)$$

where again  $Z_c$  is the normalization  $Z_c = \sum_s Z_{x_i^1=s}^{ij}$ . Detailed derivations of these relations are given in Appendix C.1.

Furthermore, each bias  $b_{x_i}^i$  is updated independently according to (24) only with probability

$$p(t) = 1 - (1 + t)^{-\gamma}, \quad (27)$$

where  $t$  is the current value of the iteration step and  $\gamma$  is an additional hyperparameter. Note that other choices of the update scheme (24) and the probability (27) exist. We adopt the scheme from [69] that provided good results in our setting.

---

**Algorithm 1** History Passing Reinforcement

 (factor graph  $(G, S, F, \{\Xi_k\}, \{\lambda_k\}, p, c)$ , steps threshold  $T_{\max}$ , damping  $\varepsilon$ , hyperparameters:  $\pi, \gamma$ )
 

---

```

Initialize uniformly at random biases  $b_{x_i}^i$  and messages  $\chi_{\underline{x}_i, \underline{x}_j}^{i \rightarrow j}$  on the factor graph and normalize them.
 $t \leftarrow 0$ 
while  $t \leq T_{\max}$  do
  Update all the messages  $\chi_{\underline{x}_i, \underline{x}_j}^{i \rightarrow j}$  according to (23) with damping  $\varepsilon$  (29).
  Compute the marginals  $\mu_{x_i^1=s}^i$  from eq. (25).
  Update each bias independently according to (24) with probability  $p(t)$  (27).
  Obtain new trial solution  $\mathbf{x}_t^{\text{sol}}$  using (28).
   $t \leftarrow t + 1$ 
end while
return  $\mathbf{x}_t^{\text{sol}}$  with lowest initial magnetization and which is a solution.
  
```

---

The BDCM probability distribution is set up so that only the graph trajectories respecting the graph dynamics have nonzero measure, and the observables can be tuned via the Lagrange parameters. Hence, by computing the marginals (25), we get estimates of the probability that each node  $i$  starts with value  $s$  under these conditions. Since biases reflect the relative values of the marginals for each node trajectory (24), we can use them to obtain our guess of a solution  $\mathbf{x}^{\text{sol}} \in S^n$ :

$$x_i^{\text{sol}} = \underset{s \in \{\pm 1\}}{\text{argmax}} b_s^i, \quad \forall i = 1, \dots, n \quad (28)$$

so  $s \in \{\pm 1\}$  with a larger bias (hence also with higher marginal) is taken as a trial solution value for given  $i$ .

After every iteration of the message update equations (23), we update the biases (24) with probability (27). This probability is low at the beginning: we essentially update the messages according to the BDCM equations and gather information towards the correct initialization of the graph. Progressively, the biases are changed in accordance with the marginals. This reinforces our beliefs about the trial solution, and if this trial solution aligns with the constraints (dynamics and initial magnetization) we get a true solution; if not, the biases continue to change, and hence also the messages until we get this alignment. Figure 11 (left) from appendix C.2 captures this development for a specific example.

To increase the stability of the algorithm during the message update (8), we introduce a damping parameter  $\varepsilon \in (0, 1)$  as follows:

$$\chi_{\underline{x}_i, \underline{x}_j}^{i \rightarrow j}(\text{final}) = \varepsilon \chi_{\underline{x}_i, \underline{x}_j}^{i \rightarrow j}(\text{after}) + (1 - \varepsilon) \chi_{\underline{x}_i, \underline{x}_j}^{i \rightarrow j}(\text{before}). \quad (29)$$

The *after* and *before* denote the message value after and before the update (8) and *final* is the final updated message value with damping.

**Generalization** The HPR procedure extends naturally beyond the present setting. It can incorporate general hard constraints on trajectory values (not limited to the attractor states considered here). Additional observables and their associated Lagrange multipliers can also be included. Furthermore, the framework applies to systems with more than two node states ( $|S| > 2$ ) and to optimization problems involving edge observables  $\bar{\Xi}$ . These generalizations require introducing additional hyperparameters  $\pi_k$  with  $\sum_k \pi_k = 1$ , otherwise the procedure remains unchanged.

**Algorithmic complexity** One iteration of HPR requires updating all messages  $\chi_{\underline{x}_i, \underline{x}_j}^{i \rightarrow j}$  according to Equation (23). On a given graph, there are  $2|E| 2^{2(p+c)}$  message values. For sparse graphs where the number of edges grows linearly with the system size  $n$ , this leads to a linear scaling with  $n$  which can easily be parallelized. However, each message update (23) goes over all trajectory combinations  $\underline{x}_{\partial i \setminus j}$ , amounting to  $2^{(d(i)-1)(p+c)}$  terms, where  $d(i)$  is the degree of node  $i$ . The marginals (26) require a sum over  $2^{2(p+c)}$  terms, while the update of the biases (24) and creation of a solution (28) again require  $\sim n$  operations which can be parallelized. This results in a complexity of  $\mathcal{O}(n 2^{(d_{\max}+1)(p+c)})$ , with an exponential dependence on  $d_{\max}, p, c$ .

$p$	$d$				
	3	4	5	6	
1	$m_{\text{sample}}^*$	0.777	0.617	0.443	0.398
	$m_{\text{HPR}}^*$	0.384(1)	0.263(9)	0.278(9)	0.231(5)
	$m_{\text{dRSB}}^*$	0.379	0.258	0.274	0.221
2	$m_{\text{sample}}^*$	0.692	0.496	0.302	0.255
	$m_{\text{HPR}}^*$	0.210(0)	0.086(9)	0.091(4)	0.049(1)
	$m_{\text{dRSB}}^*$	0.199*	0.075*	0.081*	0.039*
3	$m_{\text{sample}}^*$	0.643	0.457	0.231	0.188
	$m_{\text{SA}}^*$	0.17(1)	0.06(1)	0.04(1)	0.02(1)
	$m_{\text{HPR}}^*$	0.122(0)	-0.003(9)	-0.004(8)	-0.035(3)
	$m_{\text{dRSB}}^*$	0.117*	-0.005*	-	-

Table 3: Comparison of the best achievable  $m_{\text{init}}$  with algorithms to the threshold where typical initialization cease to evolve to a  $+1$  consensus  $m_{\text{sample}}^*$  and d1RSB threshold for  $d$ -RRG. The numbers in brackets denote the standard deviation. The values  $m_{\text{sample}}^*$  and  $m_{\text{dRSB}}^*$  are from Table 2. We ran HPR for 10,000 steps and record the best trial solution that reached consensus within  $p$  steps. Results are then averages over 10 runs on graphs of size  $n = 10,000$ . The values with an asterisk are an upper bound on the d1RSB phase, stemming from the last RS stable values of  $m_{\text{init}}$ . Also shown are the minimal values of  $m_{\text{init}}$  reached by the SA procedure. Note that *subzero* values of  $m_{\text{init}}$  correspond to states where minority becomes majority. Unlike SA, HPR is able to explicitly find such states for  $d \geq 4, p = 3$ , as predicted by the BDCM.

However, for factor nodes or dynamical rules that do not depend on the ordering of the neighbors, we can devise a dynamic programming scheme [63, 64] that eliminates the exponential dependence on  $d$ . This is the case for the majority rule (1), which depends only on the sum of the neighbors at each time step. Thus, the complexity reduces to  $\mathcal{O}(nd^{(p+c)})$ , where the main limitation comes from the exponential dependence, as the HPR equations can be solved in parallel for each message and node. Appendix C.3 describes this scheme and provides an example of dynamic programming applied to HPR updates in the setting of majority dynamics on RRGs.

## 6 HPR for Minority Takeover on Random Regular Graphs

Our goal is to find an initialization for a specific instance of a large random graph that attains the lowest possible magnetization, while reaching  $+1$  consensus within  $p$  steps. We follow the procedure described in the HPR Algorithm 1, complemented by the dynamic programming implementation in Algorithm 2, and discuss the impact of replica symmetry breaking.

Table 3 presents the minimal initial magnetization  $m_{\text{HPR}}^*$  obtained using HPR for varying degrees  $d$  and path lengths  $p$ . To obtain these values, we generate 10 random instances of  $d$ -RRG with  $n = 10^4$  nodes and perform the HPR procedure for each combination of  $d$  and  $p$ . The complete HPR parameters are listed in Table 8 in Appendix C.5. The resulting initial magnetizations leading to consensus are then averaged. In particular, for  $d \geq 4, p \geq 3$  we observe that HPR indeed finds initializations with subzero magnetization: initializations where a minority quickly turns into the majority.

The values achieved by the HPR are significantly lower than the values  $m_{\text{sample}}^*$ . We recall that  $m_{\text{sample}}^*$  denotes the threshold below which the  $+1$  consensus stops being the entropically dominating attractor, i.e. the lowest value of  $m_{\text{init}}$  for which the dynamics ends in the homogeneous attractor when initialized uniformly at random as  $n \rightarrow \infty$ . This underscores the impact of strategic initialization. Moreover, as noted in Section 2, the dynamical difference between strategic and typical initializations can be seen as an Mpemba-like effect. Using HPR, we can indeed find such initializations that are “hotter” (farther from the all-ones consensus) but nevertheless reach equilibrium faster than colder, randomly initialized states.

In Table 3 we further compare the HPR-obtained initial magnetization  $m_{\text{HPR}}^*$  with those obtained via an

alternative algorithmic strategy – simulated annealing (SA) [39]. We call the minimal initial magnetization obtained from SA  $m_{\text{SA}}^*$ . We describe the SA procedure in the context of majority dynamics on  $d$ -RRGs in Appendix D. The SA parameters are summarized in Table 9 and, due to slow convergence,  $n = 3000$  was used. Note that, for  $p = 3$ , the SA algorithm was unable to reach subzero magnetization initializations, even when the HPR was. More extensive comparison (including  $p \leq 3$ , different  $ns$  and a check of a longer path to consensus for obtained initializations) of the SA and HPR performances can be found in Appendices C, D.

The analysis above focuses on solutions whose initial configurations reach full consensus within at most  $p$  steps. However, both the HPR and SA algorithms can generate initial configurations that, while not satisfying this constraint, nonetheless converge to consensus quickly, possibly starting from even a lower  $m_{\text{init}}$ . In this sense, HPR can serve as a heuristic for identifying configurations that reach consensus after an effective time  $T_{\text{eff}} > p$ , even though the optimization only enforces behavior up to time  $p$ . We did not explore this direction systematically, since doing so would require controlling the magnetization at time  $p$ . However, we note that constraining consensus at step  $p$  alone already yields configurations that ultimately reach consensus at  $T_{\text{eff}} > p$  with initial magnetizations lower than  $m_{\text{HPR}}^*$  at time  $p$ . These additional results are presented in Appendix C.2. A similar analysis is conducted for SA in Appendix D.

The HPR approaches but does not reach the RS lower bounds  $m_{\text{RS}}^*$  (Table 2). While tuning the hyper-parameters such as  $\lambda_{\text{init}}$  allows the HPR algorithm to reach lower values of  $m_{\text{HPR}}^*$  at the cost of a larger number of steps (as shown in Figure 11), these values plateau before reaching  $m_{\text{RS}}^*$ . We discuss this next.

**1RSB implications on algorithmic performance of HPR** The Overlap Gap Property (OGP) provides a rigorous explanation for typical-case hardness and has been proven to defeat a broad class of algorithms [24]. Its key feature is a solution space of small, distant clusters, a concept related to the frozen clusters discussed in Section 4.3, which are conjectured to contain algorithmically inaccessible solutions [69, 67, 25, 70]. The frozen d1RSB phase often signals the onset of this complex geometry. We provide experimental evidence for this framework in a dynamical setting.

The lowest initial magnetization  $m_{\text{HPR}}^*$  reached by the HPR algorithm is, in all considered cases, very close to the d1RSB threshold  $m_{\text{dRSB}}^*$ , as seen in Table 3. Thus, the d1RSB transition seems to mark the limiting performance of the HPR algorithm. However, the onset of d1RSB is in general not sufficient to have generic algorithmic hardness [43]. In addition, it is postulated that the solutions must be frozen. The study of frozen clusters is discussed in Section 4.3 and expanded upon in Appendix B.5. While not conclusive, our numerical results suggest that freezing appears as soon as the d1RSB phase is entered. This is consistent with the performance of HPR. This also suggests that  $m_{\text{dRSB}}^*$  marks the initial magnetization under which initial configurations that go to consensus are hard to find algorithmically in a reasonable time.

## 7 Conclusion and Future Work

In this work, we investigated how the behavior of complex systems depends on initial conditions, focusing on synchronous discrete-time dynamics on sparse graphs. Specifically, we considered the majority dynamics of binary variables on random  $d$ -regular graphs. In this setting, we used the backtracking dynamical cavity method (BDCM) to obtain lower bounds on the initial magnetizations that lead to +1 consensus in typical  $d$ -random regular graphs in the limit where the number of nodes  $n$  goes to infinity. To find such low magnetization initializations on a given graph, we introduced the history passing reinforcement (HPR) algorithm. HPR outperforms the simulated annealing approach and reaches initializations where +1 nodes begin as a minority but, within a few steps, become the consensus for all  $d \geq 4$  random regular graphs. The existence of such configurations for random 3-regular graphs is left as an open challenge.

We complement these results with one-step replica symmetry breaking (1RSB) calculations that identify the onset of the dynamical one-step replica symmetry breaking (d1RSB) phase as an accurate marker of the performance limits of the HPR algorithm. In particular, the lowest initial magnetization values achieved by HPR consistently remain close to the d1RSB threshold. Additionally, the 1RSB analysis seems to indicate that typical solutions are frozen. Thus, we hypothesize that the d1RSB threshold marks the onset of algorithmic hardness for the considered graph ensemble. Our results advance the understanding of belief propagation based reinforcement algorithms and their limitations in the largely uncharted dynamical regime.

The HPR algorithm is based on the BDCM and thus shares the same limitations. In particular, it is computationally constrained to short trajectories (exponential complexity in the length of trajectories), and so it is also restricted to dynamical systems with short attractors. Additionally, in some settings, we observe a sensitive dependence of the required number of iterations on the hyperparameter values. To achieve optimal performance, fine-tuning of these hyperparameters is needed.

HPR demonstrably provides insights into the difficult study of non-equilibrium properties in dynamical systems. Therefore, we expect it to help address various combinatorial optimization questions in toy models of such complex phenomena as epidemics, ecology, spin glasses, and social dynamics.

Possible extensions of this work include incorporating dynamical rules that vary across individual nodes. This would lead to more realistic models of social phenomena or various bribing scenarios, where not only the initial values of nodes but also their behavior can be influenced. The effectiveness of HPR on other classes of graphs than random regular remains an open question. Thus, another avenue for future research is applying HPR to sparse real-world networks or graphs that evolve over time. Additionally, an important extension would be to consider more than two possible node values. Furthermore, we expect that the results produced by the BDCM and HPR procedures can offer insights that will aid mathematicians in devising formal proofs of the “power of few” [65, 9, 61] behavior. This could be facilitated by the fact that the replica symmetric entropy in this problem is equal to the annealed entropy that is typically simpler to treat rigorously.

## Acknowledgments

We thank Chris Moore for suggesting the name of the algorithm, Marija Vucelja and Pasquale Calabrese for insightful discussions about the connection to the Mpemba effect. We are grateful to Aude Maier for her initial explorations on understanding structured initializations in majority dynamics, which partly inspired this work. MJ would like to thank the national grid infrastructure MetaCentrum for providing computational resources, supported by the Ministry of Education, Youth and Sports of the Czech Republic (project LM2018140).

## References

- [1] Fabrizio Altarelli et al. “Optimizing spread dynamics on graphs by message passing”. In: *Journal of Statistical Mechanics: Theory and Experiment* 2013.9 (Sept. 2013). Publisher: IOP Publishing and SISSA, P09011.
- [2] Fabrizio Altarelli et al. “The patient-zero problem with noisy observations”. In: *Journal of Statistical Mechanics: Theory and Experiment* 2014.10 (Oct. 2014). Publisher: IOP Publishing and SISSA, P10016.
- [3] Erik Aurell and Hamed Mahmoudi. “A message-passing scheme for non-equilibrium stationary states”. In: *Journal of Statistical Mechanics: Theory and Experiment* 2011.4 (Apr. 2011), P04014.
- [4] Robert Axelrod. “The Dissemination of Culture: A Model with Local Convergence and Global Polarization”. In: *Journal of Conflict Resolution* 41.2 (1st Apr. 1997). Publisher: SAGE Publications Inc, pp. 203–226.
- [5] Marco Baity-Jesi et al. “The Mpemba effect in spin glasses is a persistent memory effect”. In: *Proceedings of the National Academy of Sciences* 116.31 (2019), pp. 15350–15355.
- [6] Luca Becchetti, Andrea Clementi and Emanuele Natale. “Consensus Dynamics: An Overview”. In: *ACM SIGACT News* 51.1 (12th Mar. 2020), pp. 58–104.
- [7] Freya Behrens, Barbora Hudcová and Lenka Zdeborová. “Backtracking Dynamical Cavity Method”. In: *Physical Review X* 13.3 (Aug. 2023).
- [8] Freya Behrens, Barbora Hudcová and Lenka Zdeborová. “Dynamical phase transitions in graph cellular automata”. In: *Phys. Rev. E* 109 (4 Apr. 2024), p. 044312.
- [9] Ross Berkowitz and Pat Devlin. “Central limit theorem for majority dynamics: Bribing three voters suffices”. In: *Stochastic Processes and their Applications* 146 (2022), pp. 187–206.
- [10] Hans A. Bethe. “Statistical physics of superlattices”. In: *Proc. Roy. Soc. London A* 150:552–575 (1935).

[11] Alfredo Braunstein, Louise Budzynski and Matteo Mariani. "Statistical mechanics of inference in epidemic spreading". In: *Physical Review E* 108.6 (15th Dec. 2023). Publisher: American Physical Society, p. 064302.

[12] Alfredo Braunstein and Guilhem Semerjian. "The cavity method: from exact solutions to algorithms". In: *Spin Glass Theory and Far Beyond: Replica Symmetry Breaking After 40 Years*. World Scientific, 2023, pp. 375–387.

[13] Alfredo Braunstein et al. "Encoding for the Blackwell Channel with Reinforced Belief Propagation". In: *2007 IEEE International Symposium on Information Theory*. 2007 IEEE International Symposium on Information Theory. ISSN: 2157-8117. June 2007, pp. 1891–1895.

[14] Claudio Castellano, Santo Fortunato and Vittorio Loreto. "Statistical physics of social dynamics". In: *Reviews of Modern Physics* 81.2 (11th May 2009). Publisher: American Physical Society, pp. 591–646.

[15] Joël Chavas et al. "Survey-propagation decimation through distributed local computations". In: *J Stat Mech* 2005 (30th Nov. 2005).

[16] Gennaro Cordasco et al. "Whom to befriend to influence people". In: *Theoretical Computer Science* 810 (2020). Special issue on Structural Information and Communication Complexity, pp. 26–42.

[17] Gino Del Ferraro and Erik Aurell. "Dynamic message-passing approach for kinetic spin models with reversible dynamics". In: *Physical Review E* 92.1 (21st July 2015). Publisher: American Physical Society, p. 010102.

[18] Andreas Flache et al. "Models of Social Influence: Towards the Next Frontiers". In: *Journal of Artificial Societies and Social Simulation* 20.4 (2017), p. 2.

[19] Silvio Franz and Michele Leone. "Replica bounds for optimization problems and diluted spin systems". In: *Journal of Statistical Physics* 111.3 (2003), pp. 535–564.

[20] Marylou Gabrié et al. "Phase transitions in the q-coloring of random hypergraphs". In: *Journal of Physics A: Mathematical and Theoretical* 50.50 (Nov. 2017), p. 505002.

[21] Serge Galam. "Majority rule, hierarchical structures, and democratic totalitarianism: A statistical approach". In: *Journal of Mathematical Psychology* 30.4 (1st Dec. 1986), pp. 426–434.

[22] Serge Galam. "Sociophysics: A review of Galam models". In: *International Journal of Modern Physics C* 19.03 (2008), pp. 409–440.

[23] Serge Galam. *Sociophysics: A Physicist's Modeling of Psycho-political Phenomena*. Understanding Complex Systems. Boston, MA: Springer US, 2012.

[24] David Gamarnik. "The overlap gap property: A topological barrier to optimizing over random structures". In: *Proceedings of the National Academy of Sciences* 118.41 (Oct. 2021).

[25] David Gamarnik, Christopher Moore and Lenka Zdeborová. "Disordered systems insights on computational hardness". In: *Journal of Statistical Mechanics: Theory and Experiment* 2022.11 (Nov. 2022), p. 114015.

[26] Bernd Gärtner and Ahad N. Zehmakan. "Majority Model on Random Regular Graphs". In: *LATIN 2018: Theoretical Informatics*. Ed. by Michael A. Bender, Martín Farach-Colton and Miguel A. Mosteiro. Cham: Springer International Publishing, 2018, pp. 572–583.

[27] Davide Ghio et al. "Bayes-optimal inference for spreading processes on random networks". In: *Physical Review E* 108.4 (16th Oct. 2023). Publisher: American Physical Society, p. 044308.

[28] Eric Goles-Chacc, Françoise Fogelman-Soulie and Didier Pellegrin. "Decreasing energy functions as a tool for studying threshold networks". In: *Discrete Applied Mathematics* 12.3 (1985), pp. 261–277.

[29] Michel Grabisch and Agnieszka Rusinowska. "A Survey on Nonstrategic Models of Opinion Dynamics". In: *Games* 11.4 (Dec. 2020). Number: 4 Publisher: Multidisciplinary Digital Publishing Institute, p. 65.

[30] Mark Granovetter. "Threshold Models of Collective Behavior". In: *American Journal of Sociology* 83.6 (May 1978), pp. 1420–1443.

[31] Alberto Guggiola and Guilhem Semerjian. "Minimal Contagious Sets in Random Regular Graphs". In: *Journal of Statistical Physics* 158.2 (Oct. 2014), pp. 300–358.

[32] Wilfred K. Hastings. “Monte Carlo sampling methods using Markov chains and their applications”. In: *Biometrika* 57.1 (Apr. 1970), pp. 97–109.

[33] Gregory Herschlag et al. “Quantifying gerrymandering in north carolina”. In: *Statistics and Public Policy* 7.1 (2020), pp. 30–38.

[34] Sungmin Hwang et al. “On the Number of Limit Cycles in Diluted Neural Networks”. In: *Journal of Statistical Physics* 181.6 (1st Dec. 2020), pp. 2304–2321.

[35] Monwhea Jeng. “The Mpemba effect: When can hot water freeze faster than cold?” In: *American Journal of Physics* 74.6 (2006), pp. 514–522.

[36] Yashodhan Kanoria and Andrea Montanari. “Majority dynamics on trees and the dynamic cavity method”. In: *The Annals of Applied Probability* 21.5 (Oct. 2011). Publisher: Institute of Mathematical Statistics, pp. 1694–1748.

[37] Brian Karrer and Mark E. J. Newman. “Message passing approach for general epidemic models”. In: *Physical Review E* 82.1 (2nd July 2010). Publisher: American Physical Society, p. 016101.

[38] David Kempe, Jon Kleinberg and Éva Tardos. “Maximizing the spread of influence through a social network”. In: *Proceedings of the Ninth ACM SIGKDD International Conference on Knowledge Discovery and Data Mining*. KDD ’03. Washington, D.C.: Association for Computing Machinery, 2003, pp. 137–146.

[39] Scott Kirkpatrick, C. Daniel Gelatt Jr and Mario P. Vecchi. “Optimization by Simulated Annealing”. In: *Science* 220.4598 (1983), pp. 671–680.

[40] Israel Klich et al. “Mpemba index and anomalous relaxation”. In: *Physical Review X* 9.2 (2019), p. 021060.

[41] Cédric Koller, Freya Behrens and Lenka Zdeborová. “Counting and hardness-of-finding fixed points in cellular automata on random graphs”. In: *Journal of Physics A: Mathematical and Theoretical* 57.46 (Nov. 2024), p. 465001.

[42] Florent Krzakala and Lenka Zdeborová. *Statistical Physics Methods in Optimization and Machine Learning*. Lecture notes, 2021.

[43] Florent Krzakala et al. “Gibbs States and the Set of Solutions of Random Constraint Satisfaction Problems”. In: *Proceedings of the National Academy of Sciences* 104.25 (19th June 2007), pp. 10318–10323.

[44] Avinash Kumar and John Bechhoefer. “Exponentially faster cooling in a colloidal system”. In: *Nature* 584.7819 (2020), pp. 64–68.

[45] Andrey Y. Lokhov, Marc Mézard and Lenka Zdeborová. “Dynamic message-passing equations for models with unidirectional dynamics”. In: *Physical Review E* 91.1 (13th Jan. 2015). Publisher: American Physical Society, p. 012811.

[46] Zhiyue Lu and Oren Raz. “Nonequilibrium thermodynamics of the Markovian Mpemba effect and its inverse”. In: *Proceedings of the National Academy of Sciences* 114.20 (2017), pp. 5083–5088.

[47] Nicholas Metropolis et al. “Equation of State Calculations by Fast Computing Machines”. In: *Journal of Chemical Physics* 21 (1953), pp. 1087–1092.

[48] Marc Mézard and Andrea Montanari. “Reconstruction on Trees and Spin Glass Transition”. In: *J. Stat. Phys.* 124.6 (2006), pp. 1317–1350.

[49] Marc Mézard and Andrea Montanari. *Information, Physics, and Computation*. Oxford University Press, Jan. 2009.

[50] Marc Mézard and Giorgio Parisi. “The Bethe lattice spin glass revisited”. In: *The European Physical Journal B* 20.2 (Mar. 2001), pp. 217–233.

[51] Marc Mézard and Giorgio Parisi. “The cavity method at zero temperature”. In: *Journal of Statistical Physics* 111 (2003). 22 pages, 8 figures; Some minor corrections, pp. 1–34.

[52] Marc Mézard, Giorgio Parisi and Miguel A. Virasoro. “SK Model: The Replica Solution without Replicas”. In: *Europhysics Letters* 1.2 (Jan. 1986), p. 77.

[53] Marc Mézard, Giorgio Parisi and Miguel Angel Virasoro. *Spin glass theory and beyond: An Introduction to the Replica Method and Its Applications*. Vol. 9. World Scientific Publishing Company, 1987.

[54] Marc Mézard, Giorgio Parisi and Riccardo Zecchina. “Analytic and Algorithmic Solution of Random Satisfiability Problems”. In: *Science* 297.5582 (2nd Aug. 2002), pp. 812–815.

[55] Andrea Montanari, Federico Ricci-Tersenghi and Guilhem Semerjian. “Clusters of solutions and replica symmetry breaking in random k-satisfiability”. In: *Journal of Statistical Mechanics: Theory and Experiment* 2008.4 (Apr. 2008), P04004.

[56] Erasto B. Mpemba and Denis G. Osborne. “Cool?” In: *Physics Education* 4.3 (1969), pp. 172–175.

[57] Izaac Neri and Désiré Bollé. “The cavity approach to parallel dynamics of Ising spins on a graph”. In: *Journal of Statistical Mechanics: Theory and Experiment* 2009.8 (Aug. 2009), P08009.

[58] Giorgio Parisi. “Order Parameter for Spin-Glasses”. In: *Phys. Rev. Lett.* 50 (24 June 1983), pp. 1946–1948.

[59] Judea Pearl. *Reverend Bayes on Inference Engines: A Distributed Hierarchical Approach*. Association for Computing Machinery, Aug. 1982, pp. 123–136.

[60] David Saad et al. “Physics-inspired methods for networking and communications”. In: *IEEE Communications Magazine* 52.11 (Nov. 2014). Conference Name: IEEE Communications Magazine, pp. 144–151.

[61] Ashwin Sah and Mehtaab Sawhney. “Majority dynamics: The power of one”. In: *Israel Journal of Mathematics* 267.1 (2025), pp. 85–133.

[62] Katarzyna Sznajd-Weron and Józef Sznajd. “Opinion evolution in closed community”. In: *International Journal of Modern Physics C* 11.6 (Sept. 2000). Publisher: World Scientific Publishing Co., pp. 1157–1165.

[63] Giuseppe Torrisi, Alessia Annibale and Reimer Kühn. “Overcoming the complexity barrier of the dynamic message-passing method in networks with fat-tailed degree distributions”. In: *Phys. Rev. E* 104 (4 Oct. 2021), p. 045313.

[64] Giuseppe Torrisi, Reimer Kühn and Alessia Annibale. “Uncovering the non-equilibrium stationary properties in sparse Boolean networks”. In: *Journal of Statistical Mechanics: Theory and Experiment* 2022.5 (May 2022), p. 053303.

[65] Linh Tran and Van Vu. “Reaching a consensus on random networks: the power of few”. In: *Approximation, Randomization, and Combinatorial Optimization. Algorithms and Techniques (APPROX/RANDOM 2020)*. Schloss Dagstuhl–Leibniz-Zentrum für Informatik. 2020, pp. 20–1.

[66] Haoxiang Xia, Huili Wang and Zhaoguo Xuan. “Opinion Dynamics: A Multidisciplinary Review and Perspective on Future Research”. In: *International Journal of Knowledge and Systems Science (IJKSS)* 2.4 (2011). Publisher: IGI Global, pp. 72–91.

[67] Lenka Zdeborová. *Statistical Physics of Hard Optimization Problems*. 2008.

[68] Lenka Zdeborová and Florent Krzakala. “Phase transitions in the coloring of random graphs”. In: *Physical Review E* 76.3 (Sept. 2007).

[69] Lenka Zdeborová and Marc Mézard. “Constraint satisfaction problems with isolated solutions are hard”. In: *Journal of Statistical Mechanics: Theory and Experiment* 2008.12 (8th Dec. 2008), P12004.

[70] Lenka Zdeborová and Marc Mézard. “Locked Constraint Satisfaction Problems”. In: *Physical Review Letters* 101.7 (2008), p. 078702.

[71] Abdolahad N. Zehmakan. “On the Spread of Information through Graphs”. PhD thesis. ETH Zurich, 2019.

[72] Ahad N. Zehmakan. “Majority Opinion Diffusion in Social Networks: An Adversarial Approach”. In: *Proceedings of the AAAI Conference on Artificial Intelligence* 35 (18th May 2021), pp. 5611–5619.

[73] Ahad N. Zehmakan. “On the spread of influence in graphs”. In: *Information and Computation* 281 (1st Dec. 2021), p. 104808.

## A Derivation of the BDCM relations

**Factor graph and BDCM equations.** In the main text, we have defined a probability distribution over graph trajectories  $\underline{\mathbf{x}}$  in equation (2). We have also shown how this probability distribution factorizes into (7) by leveraging the locality of the dynamical rule  $f_i : S \times S^{|\partial i|} \rightarrow S$  and the observables  $\tilde{\Xi}(\underline{x}_i) : S^{p+c} \rightarrow \mathbb{R}$ ,  $\tilde{\Xi}(\underline{x}_i, \underline{x}_j) : S^{2(p+c)} \rightarrow \mathbb{R}$ . We repeat the factorized form of the backtracking dynamical cavity method (BDCM) probability distribution here for convenience:

$$P(\underline{\mathbf{x}}) = \frac{1}{Z} \prod_{i \in V} \underbrace{\left[ e^{-\sum_{\bar{k}} \lambda_{\bar{k}} \tilde{\Xi}_{\bar{k}}(\underline{x}_i)} \mathbb{1} \left[ x_i^{p+1} = f_i(x_i^{p+c}, \mathbf{x}_{\partial i}^{p+c}) \right] \prod_{t=1}^{p+c-1} \mathbb{1} \left[ x_i^{t+1} = f_i(x_i^t, \mathbf{x}_{\partial i}^t) \right] \right]}_{\mathcal{A}_i(\underline{x}_i, \mathbf{x}_{\partial i})} \prod_{(ij) \in E} \underbrace{\left[ e^{-\sum_{\bar{k}} \lambda_{\bar{k}} \tilde{\Xi}_{\bar{k}}(\underline{x}_i, \underline{x}_j)} \right]}_{a(\underline{x}_i, \underline{x}_j)}. \quad (30)$$

Now, we describe how we can graphically represent this probability distribution and arrive at the BDCM equations (8), which are used to obtain an estimate of the free entropy density  $\Phi = \log Z/n$ . We recall that  $Z$  is the normalization/partition function such that  $P(\underline{\mathbf{x}})$  is a proper probability distribution.

We start by assuming that the graph  $G$  is a *tree* and construct a naive *factor graph*, where the node values  $\{\underline{x}_i\}, i \in V$  are present as *variable nodes*, and the functions  $\{\mathcal{A}_i(\underline{x}_i, \mathbf{x}_{\partial i})\}, i \in V$  and  $\{a(\underline{x}_i, \underline{x}_j)\}, (ij) \in E$  are represented as *factor nodes*. In the factor graph, there is an edge between a variable node and a factor node if and only if the variable  $\underline{x}_i$  is among the arguments of the corresponding factor function. Hence, the factor graph is bipartite. This straightforward construction of the factor graph is depicted in Figure 4 (middle). We can see that the factor graph constructed in this way does not preserve the tree structure of the original graph  $G$ . This construction introduces many short cycles, which is generally problematic for belief propagation (BP) procedures. We remedy this by introducing new variable nodes, the pairs of trajectories  $\{(\underline{x}_i, \underline{x}_j)\}, (ij) \in E$ . Now, in place of *edges* in the original graph  $G$ , we have variable *nodes*  $\{(\underline{x}_i, \underline{x}_j)\}$  and their corresponding factor nodes  $\{a(\underline{x}_i, \underline{x}_j)\}$ , which are attached only to these variable nodes. In place of the nodes of  $G$ , we have the factor nodes  $\{\mathcal{A}_i(\underline{x}_i, \mathbf{x}_{\partial i})\}$ . Hence, we refer to this construction as the factor graph in the *edge-dual* representation of the graph  $G$ . We denote by  $ij = ji$  the variable nodes  $(\underline{x}_i, \underline{x}_j)$ , and by  $\partial ij$  a set of factor nodes that share an edge with the variable node  $ij$ , *except* the factor node  $a(\underline{x}_i, \underline{x}_j)$ . Hence,  $\partial ij$  is composed of the two factor nodes  $\mathcal{A}_i(\underline{x}_i, \mathbf{x}_{\partial i})$  and  $\mathcal{A}_j(\underline{x}_j, \mathbf{x}_{\partial j})$ . The factor nodes  $\mathcal{A}_i(\underline{x}_i, \mathbf{x}_{\partial i})$  are denoted as  $A_i$ , and we write as  $\partial A_i$  the set of variable nodes on which the factor node acts. We summarize this in Table 4.

Factor graph node	Type	Symbol	Neighborhood	Neib. symbol
$\mathcal{A}_i(\underline{x}_i, \mathbf{x}_{\partial i})$	function	$A_i$	$\{(\underline{x}_i, \underline{x}_j)\}_{j \in \partial i}$	$\partial A_i$
$a(\underline{x}_i, \underline{x}_j)$	function	$a_{ij} = a_{ji}$	$(\underline{x}_i, \underline{x}_j)$	$\partial a_{ij}$
$(\underline{x}_i, \underline{x}_j)$	variable	$ij = ji$	$\mathcal{A}_i(\underline{x}_i, \mathbf{x}_{\partial i}), \mathcal{A}_j(\underline{x}_j, \mathbf{x}_{\partial j})$	$\partial ij$

Table 4: The factor graph is a bipartite graph with variable and factor nodes. This table summarizes the definitions and abbreviations used in the BDCM context.

This construction of the factor graph preserves the tree structure of  $G$ , which plays an important role in the procedure for iterative computation of the normalization  $Z$ .

Choosing a factor node  $\mathcal{A}_i(\underline{x}_i, \mathbf{x}_{\partial i})$  for arbitrary  $i \in G$  and rooting the factor graph in it, we can write the normalization  $Z$  as

$$\begin{aligned} Z &= \sum_{\{\underline{\mathbf{x}}\}} P(\underline{\mathbf{x}}) = \sum_{\{\underline{\mathbf{x}}\}_G} \prod_{i \in G} \mathcal{A}_i(\underline{x}_i, \mathbf{x}_{\partial i}) \prod_{(ij) \in G} a(\underline{x}_i, \underline{x}_j) = \\ &= \sum_{\{\underline{x}_i, \mathbf{x}_{\partial i}\}} \mathcal{A}_i(\underline{x}_i, \mathbf{x}_{\partial i}) \prod_{ij \in \partial A_i} \left( \sum_{\{\underline{\mathbf{x}}\}_{G_{ij}} \setminus \{\underline{x}_i, \underline{x}_j\}} \prod_{k \in G_{ij}} \mathcal{A}_k(\underline{x}_k, \mathbf{x}_{\partial k}) \prod_{(kl) \in G_{ij}} a(\underline{x}_k, \underline{x}_l) \right). \end{aligned} \quad (31)$$

In the last equality, we use the tree structure of the factor graph to write the rest of the partition function as a product over the tree branches that stem from  $\mathcal{A}_i(\underline{x}_i, \mathbf{x}_{\partial i})$ . We denote these neighboring branches as

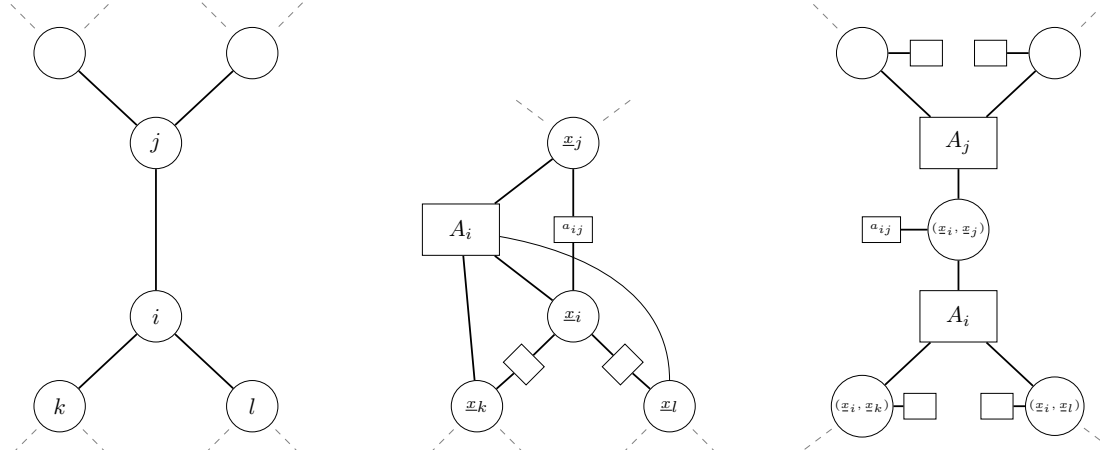


Figure 4: Factor graph construction for the BDCM probability distribution. (Left.) Part of the original tree graph  $G$ . (Middle.) Naive construction of the factor graph, where variable nodes (circles) correspond directly to the nodes of  $G$ . The addition of factor nodes in this manner produces short cycles which is problematic for the BP procedure. (Right.) Factor graph in the edge-dual representation of the graph  $G$  with pairs of trajectories  $(\underline{x}_i, \underline{x}_j)$  as variable nodes. This construction preserves the tree structure.

$\{G_{ij}\}$ ,  $ij \in \partial A_i$ , when the branch *starts* with the variable node  $(\underline{x}_i, \underline{x}_j)$  (it does not include  $A_i$ ).  $\{\underline{x}\}_{G_{ij}}$  designates the ensemble of all graph trajectories restricted to the subgraph  $G_{ij}$ . For a graphical depiction of this, see Figure 5. Note that what truly makes these branches independent is the fact that the values of the variable nodes  $(\underline{x}_i, \underline{x}_j)$ , for  $ij \in \partial A_i$  are fixed – the sum over these values is in front of the entire product. The rest of the values of the variable nodes in  $G_{ij}$ , i.e.  $\{\underline{x}\}_{G_{ij}} \setminus \{(\underline{x}_i, \underline{x}_j)\}$ , can be summed independently in all branches  $ij \in \partial A_i$ . We refer to the independent sums through these branches – taken with the fixed variable node value  $(\underline{x}_i, \underline{x}_j)$  in (31) – as *partial partition functions*, and denote them by  $V_{\underline{x}_i, \underline{x}_j}^{ij \rightarrow A_i}$ . Thus, we write (31) as

$$Z = \sum_{\{\underline{x}_i, \underline{x}_{\partial i}\}} \mathcal{A}_i(\underline{x}_i, \underline{x}_{\partial i}) \prod_{ij \in \partial A_i} V_{\underline{x}_i, \underline{x}_j}^{ij \rightarrow A_i}. \quad (32)$$

Note that  $V_{\underline{x}_i, \underline{x}_j}^{ij \rightarrow A_i}$  “goes” from a variable node to a factor node. The subscript indicates the fixed value of the variable node  $(\underline{x}_i, \underline{x}_j)$ . Let us examine the structure of the partial partition functions  $V_{\underline{x}_i, \underline{x}_j}^{ij \rightarrow A_i}$ . We can take the factor node  $a(\underline{x}_i, \underline{x}_j)$  outside the sum because the values of the variable node  $ij$  are fixed:

$$V_{\underline{x}_i, \underline{x}_j}^{ij \rightarrow A_i} = a(\underline{x}_i, \underline{x}_j) \sum_{\{\underline{x}\}_{G_{ij}} \setminus \{(\underline{x}_i, \underline{x}_j)\}} \prod_{k \in G_{ij}} \mathcal{A}_k(\underline{x}_k, \underline{x}_{\partial k}) \prod_{(kl) \in G_{ij} \setminus (ij)} a(\underline{x}_k, \underline{x}_l). \quad (33)$$

By doing so, we recognize that we are summing only over variable node values of a graph rooted at  $A_j$  (see Figure 5). We denote this graph rooted at  $A_j$  by  $G_{A_j}$ , and introduce another partial partition function going from factor node to variable node with fixed variable node value  $(\underline{x}_i, \underline{x}_j)$ :

$$R_{\underline{x}_j, \underline{x}_i}^{A_j \rightarrow ij} = \sum_{\{\underline{x}\}_{G_{A_j}}} \prod_{k \in G_{A_j}} \mathcal{A}_k(\underline{x}_k, \underline{x}_{\partial k}) \prod_{(kl) \in G_{A_j} \setminus (ij)} a(\underline{x}_k, \underline{x}_l). \quad (34)$$

We immediately have

$$V_{\underline{x}_i, \underline{x}_j}^{ij \rightarrow A_i} = a(\underline{x}_i, \underline{x}_j) R_{\underline{x}_j, \underline{x}_i}^{A_j \rightarrow ij}. \quad (35)$$

Note that the values of  $(\underline{x}_i, \underline{x}_j)$  in  $R_{\underline{x}_j, \underline{x}_i}^{A_j \rightarrow ij}$  are present in the factor node  $A_j$ , in which we rooted the graph  $G_{A_j}$ . Additionally, the fixed value of  $\underline{x}_j$  also partially fixes the variable nodes  $(\underline{x}_k, \underline{x}_j) = kj \in A_j \setminus ij$ . Therefore, similarly as above for  $Z$ , we write  $R_{\underline{x}_j, \underline{x}_i}^{A_j \rightarrow ij}$  as

$$R_{\underline{x}_j, \underline{x}_i}^{A_j \rightarrow ij} = \sum_{\{\underline{x}_{\partial j \setminus i}\}} \mathcal{A}_j(\underline{x}_j, \underline{x}_{\partial j}) \prod_{jk \in \partial A_j \setminus ij} \left( a(\underline{x}_j, \underline{x}_k) \sum_{\{\underline{x}\}_{G_{jk}} \setminus \{(\underline{x}_j, \underline{x}_k)\}} \prod_{l \in G_{jk}} \mathcal{A}_l(\underline{x}_l, \underline{x}_{\partial l}) \prod_{(lm) \in G_{jk} \setminus (jk)} a(\underline{x}_l, \underline{x}_m) \right), \quad (36)$$

where  $G_{jk}$  is defined as before with  $G_{ij}$  and is also depicted in Figure 5. We recognize (33) in (36) and get

$$R_{\underline{x}_j, \underline{x}_i}^{A_j \rightarrow ij} = \sum_{\{\underline{x}_{\partial j \setminus i}\}} \mathcal{A}_j(\underline{x}_j, \underline{x}_{\partial j}) \prod_{jk \in \partial A_j \setminus ij} V_{\underline{x}_j, \underline{x}_k}^{jk \rightarrow A_j}. \quad (37)$$

Substitution of (37) into (35) results in an iterative scheme for obtaining values of the partial partition functions  $V$ :

$$V_{\underline{x}_i, \underline{x}_j}^{ij \rightarrow A_i} = a(\underline{x}_i, \underline{x}_j) \sum_{\{\underline{x}_{\partial j \setminus i}\}} \mathcal{A}_j(\underline{x}_j, \underline{x}_{\partial j}) \prod_{jk \in \partial A_j \setminus ij} V_{\underline{x}_j, \underline{x}_k}^{jk \rightarrow A_j}. \quad (38)$$

Partition functions typically grow exponentially with  $n$ , as they are a sum over an exponential number of

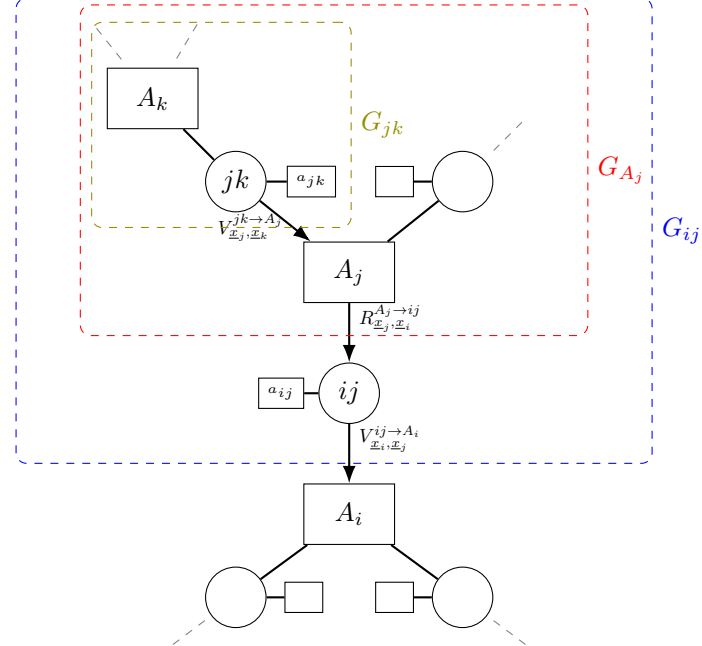


Figure 5: Derivation of the BP scheme in the BDCM setting. The tree structure of the factor graph is utilized to rewrite partition function  $Z$  via the partial partition functions  $V$  and  $R$ , for which we obtain the local iterative schemes (35) and (37).

terms. Then the iterative scheme (38) tends to be numerically unstable and it is better to transition to normalized *messages*

$$\chi_{\underline{x}_i, \underline{x}_j}^{i \rightarrow j} = \frac{V_{\underline{x}_i, \underline{x}_j}^{ij \rightarrow A_j}}{\sum_{\{\underline{x}'_i, \underline{x}'_j\}} V_{\underline{x}'_i, \underline{x}'_j}^{ij \rightarrow A_j}}. \quad (39)$$

We use the convention that  $i \rightarrow j$  designates a message that begins in variable node  $ij$  and goes in the direction of the factor node  $A_j$ . Thus, within this convention, we refer only to the nodes of the original graph  $G$ . The message  $\chi_{\underline{x}_i, \underline{x}_j}^{i \rightarrow j}$  is the probability that the variable node  $ij$  takes the value  $\underline{x}_i, \underline{x}_j$  when restricted to subgraph  $G_{ji}$  (the subgraph does not include  $A_j$ ). This is the probability in the presence of a cavity – hence the name cavity method [42].

We use the iterative scheme for the Vs to write

$$\begin{aligned}
\chi_{\underline{x}_i, \underline{x}_j}^{i \rightarrow j} &\stackrel{(39) \& (38)}{=} \frac{a(\underline{x}_i, \underline{x}_j) \sum_{\{\underline{x}_{\partial i \setminus j}\}} \mathcal{A}_i(\underline{x}_i, \underline{x}_{\partial i}) \prod_{ik \in \partial A_i \setminus ij} V_{\underline{x}_k, \underline{x}_i}^{ik \rightarrow A_i}}{\sum_{\{\underline{x}_i, \underline{x}_j\}} a(\underline{x}_i, \underline{x}_j) \sum_{\{\underline{x}_{\partial i \setminus j}\}} \mathcal{A}_i(\underline{x}_i, \underline{x}_{\partial i}) \prod_{ik \in \partial A_i \setminus ij} V_{\underline{x}_k, \underline{x}_i}^{ik \rightarrow A_i}} \cdot \frac{\prod_{ik \in \partial A_i \setminus ij} \sum_{\{\underline{x}'_k, \underline{x}'_i\}} V_{\underline{x}'_k, \underline{x}'_i}^{ik \rightarrow A_i}}{\prod_{ik \in \partial A_i \setminus ij} \sum_{\{\underline{x}'_k, \underline{x}'_i\}} V_{\underline{x}'_k, \underline{x}'_i}^{ik \rightarrow A_i}} \\
&= \frac{a(\underline{x}_i, \underline{x}_j) \sum_{\{\underline{x}_{\partial i \setminus j}\}} \mathcal{A}_i(\underline{x}_i, \underline{x}_{\partial i}) \prod_{ik \in \partial A_i \setminus ij} \frac{V_{\underline{x}_k, \underline{x}_i}^{ik \rightarrow A_i}}{\sum_{\{\underline{x}'_k, \underline{x}'_i\}} V_{\underline{x}'_k, \underline{x}'_i}^{ik \rightarrow A_i}}}{\sum_{\{\underline{x}_i, \underline{x}_j\}} a(\underline{x}_i, \underline{x}_j) \sum_{\{\underline{x}_{\partial i \setminus j}\}} \mathcal{A}_i(\underline{x}_i, \underline{x}_{\partial i}) \prod_{ik \in \partial A_i \setminus ij} \frac{V_{\underline{x}_k, \underline{x}_i}^{ik \rightarrow A_i}}{\sum_{\{\underline{x}'_k, \underline{x}'_i\}} V_{\underline{x}'_k, \underline{x}'_i}^{ik \rightarrow A_i}}}. \tag{40}
\end{aligned}$$

Writing  $ik \in A_i \setminus ij$  as  $k \in \partial i \setminus j$ , we obtain the BDCM equations (8)

$$\chi_{\underline{x}_i, \underline{x}_j}^{i \rightarrow j} = \frac{1}{Z^{i \rightarrow j}} a(\underline{x}_i, \underline{x}_j) \sum_{\{\underline{x}_{\partial i \setminus j}\}} \mathcal{A}_i(\underline{x}_i, \underline{x}_{\partial i}) \prod_{k \in \partial i \setminus j} \chi_{\underline{x}_k, \underline{x}_i}^{k \rightarrow i}, \tag{41}$$

where

$$Z^{i \rightarrow j} = \sum_{\{\underline{x}_i, \underline{x}_j\}} a(\underline{x}_i, \underline{x}_j) \sum_{\{\underline{x}_{\partial i \setminus j}\}} \mathcal{A}_i(\underline{x}_i, \underline{x}_{\partial i}) \prod_{k \in \partial i \setminus j} \chi_{\underline{x}_k, \underline{x}_i}^{k \rightarrow i}. \tag{42}$$

**Bethe free entropy density.** Knowing the values of the messages  $\chi_{\underline{x}_i, \underline{x}_j}^{i \rightarrow j}$  at a fixed point, we can compute various local quantities of interest, such as the marginal probabilities of node trajectories. We can also obtain global quantities, such as the free entropy density  $\Phi$ . In tree graphs, estimates based on the messages are exact. We continue our discussion keeping the assumption that  $G$  is a tree. We begin by writing the partition function as in (32):

$$Z = \sum_{\{\underline{x}_i, \underline{x}_{\partial i}\}} \mathcal{A}_i(\underline{x}_i, \underline{x}_{\partial i}) \prod_{ij \in \partial A_i} V_{\underline{x}_i, \underline{x}_j}^{ij \rightarrow A_i} \stackrel{(39)}{=} \left( \sum_{\{\underline{x}_i, \underline{x}_{\partial i}\}} \mathcal{A}_i(\underline{x}_i, \underline{x}_{\partial i}) \prod_{ij \in \partial A_i} \chi_{\underline{x}_j, \underline{x}_i}^{j \rightarrow i} \right) \left( \prod_{ij \in \partial A_i} \sum_{\{\underline{x}'_i, \underline{x}'_j\}} V_{\underline{x}'_i, \underline{x}'_j}^{ij \rightarrow A_i} \right). \tag{43}$$

The expression inside the first parentheses serves as a definition for the quantity  $Z^i$ :

$$Z^i = \sum_{\{\underline{x}_i, \underline{x}_{\partial i}\}} \mathcal{A}_i(\underline{x}_i, \underline{x}_{\partial i}) \prod_{j \in \partial i} \chi_{\underline{x}_j, \underline{x}_i}^{j \rightarrow i}, \tag{44}$$

where we use the same notation as above for  $ij \in \partial A_i$ . This is the definition (10) in the main text.

Now, we would like to express the terms in the second parentheses in (43) through expression involving only the messages  $\{\chi\}$ , and not the partial partition functions  $\{V\}$ . However, looking at the definition (39) of the messages  $\chi$ , we see that this effort is quite futile, as replacing the sum of Vs introduces another  $V$ . Instead, we utilize the following relation for  $Z^{i \rightarrow j}$ :

$$Z^{i \rightarrow j} = \sum_{\{\underline{x}_i, \underline{x}_j\}} a(\underline{x}_i, \underline{x}_j) \sum_{\{\underline{x}_{\partial i \setminus j}\}} \mathcal{A}_i(\underline{x}_i, \underline{x}_{\partial i}) \prod_{ik \in \partial A_i \setminus ij} \chi_{\underline{x}_k, \underline{x}_i}^{k \rightarrow i} \stackrel{(39) \& (38)}{=} \frac{\sum_{\{\underline{x}_i, \underline{x}_j\}} V_{\underline{x}_i, \underline{x}_j}^{ij \rightarrow A_j}}{\prod_{ik \in \partial A_i \setminus ij} \sum_{\{\underline{x}'_k, \underline{x}'_i\}} V_{\underline{x}'_k, \underline{x}'_i}^{ik \rightarrow A_i}}. \tag{45}$$

This gives a recurrent procedure for replacing  $\sum_{\{\underline{x}'_k, \underline{x}'_i\}} V_{\underline{x}'_k, \underline{x}'_i}^{ik \rightarrow A_i}$  with  $Z^{j \rightarrow i} \prod_{jk \in \partial A_j \setminus ij} \sum_{\{\underline{x}'_k, \underline{x}'_j\}} V_{\underline{x}'_k, \underline{x}'_j}^{jk \rightarrow A_j}$ . Hence, we write (43) as

$$Z \stackrel{(45)}{=} Z^i \prod_{ij \in \partial A_i} \left( Z^{j \rightarrow i} \prod_{jk \in \partial A_j \setminus ij} \sum_{\{\underline{x}'_k, \underline{x}'_j\}} V_{\underline{x}'_k, \underline{x}'_j}^{jk \rightarrow A_j} \right) \stackrel{(45)}{=} Z^i \prod_{ij \in \partial A_i} \left[ Z^{j \rightarrow i} \prod_{jk \in \partial A_j \setminus ij} \left( Z^{k \rightarrow j} \prod_{kl \in \partial A_k \setminus jk} \dots \right) \right]. \tag{46}$$

In equation (46) (in fact, already in (43)), we rooted the factor graph at an *arbitrary* factor node  $A_i$ . We see that (46) follows the factor graph structure. We “go” from  $A_i$  via its neighboring edges to factor nodes  $A_j$ , and then follow their neighboring edges (except the ones from which we arrived) and so on, going through the entire factor graph. This nested evaluation pattern is perhaps seen even better if we

lighten the notation using the convention introduced above. In this form, the partition function reads  $Z = Z^i \prod_{j \in \partial i} \left[ Z^{j \rightarrow i} \prod_{k \in \partial j \setminus i} \left( Z^{k \rightarrow j} \prod_{l \in \partial k \setminus j} \dots \right) \right]$ . Since the factor graph is a tree, this recurrent process ends in leaves, where partial partition functions or messages are readily evaluated (for example,  $R^{A_{\text{leaf}} \rightarrow ab} = \mathcal{A}_{\text{leaf}}(\underline{x}_a, \underline{x}_b)$  and  $V_{\underline{x}_a, \underline{x}_b}^{ab \rightarrow A_{\text{leaf}}} = a(\underline{x}_a, \underline{x}_b) \mathcal{A}_{\text{leaf}}(\underline{x}_a, \underline{x}_b)$ ).

Finally, we replace the normalizations  $Z^{j \rightarrow i}$  with another quantity that is also expressed via the messages  $\chi$ , but it is undirected. For that we introduce  $Z^{ij} = Z^{ji}$  as in (11):

$$Z^{ij} = \sum_{\{\underline{x}_i, \underline{x}_j\}} \frac{1}{a(\underline{x}_i, \underline{x}_j)} \chi_{\underline{x}_i, \underline{x}_j}^{i \rightarrow j} \chi_{\underline{x}_j, \underline{x}_i}^{j \rightarrow i} = \frac{Z^i}{Z^{i \rightarrow j}} = \frac{Z^j}{Z^{j \rightarrow i}}, \quad (47)$$

where we used the BDCM update equation (41) to rewrite one of the messages and the definition of  $Z^i$ , equation (44). Hence, we arrive at

$$\begin{aligned} Z &= Z^i \prod_{j \in \partial i} \left[ Z^{j \rightarrow i} \prod_{k \in \partial j \setminus i} \left( Z^{k \rightarrow j} \prod_{l \in \partial k \setminus j} \dots \right) \right] \stackrel{(47)}{=} Z^i \prod_{j \in \partial i} \left[ \frac{Z^j}{Z^{ij}} \prod_{k \in \partial j \setminus i} \left( \frac{Z^k}{Z^{jk}} \prod_{l \in \partial k \setminus j} \dots \right) \right] \\ &= \frac{\prod_{i \in V} Z^i}{\prod_{(ij) \in E} Z^{ij}}. \end{aligned} \quad (48)$$

From this we obtain the relation for the Bethe free entropy density (9) as

$$\Phi_B = \frac{\log Z}{n} = \frac{1}{n} \left( \sum_{i \in V} \log Z^i - \sum_{(ij) \in E} \log Z^{ij} \right). \quad (49)$$

The term in the first sum expresses the change in  $Z$  when factor node  $A_i$  (and the corresponding edges) is added to the system. The term in the second sum corresponds to the change in  $Z$  that results from the addition of the edge  $(ij)$ . Together, this describes the Bethe free entropy (49) as a sum of ‘site’ free entropies  $\Phi_i = \log Z^i$  for all  $i$  minus a correction due to a double summation over the edges. Hence, we need to subtract the ‘edge’ free entropies  $\Phi_{ij} = \log Z^{ij}$  for all edges  $(ij)$  [42].

**BP on general graphs.** We based the entire formulation of the BDCM equations (41) and the Bethe free entropy (49) on the assumption that the original graph  $G$  is a tree graph. In this setting, the derived formulas are exact. However, it was realized that applying the BP procedures on locally tree-like graphs can lead to correct results [49, 42]. We note here that random regular graphs (RRGs) are examples of a setting where using the BP procedure can lead to exact results, as these graphs typically do not contain short loops. In this general setting, we initialize the messages randomly and iterate the BDCM equations until convergence rather than evaluating the messages from leaves to the root and back.

More generally, BP procedures on general graphs are exact when the following holds: removing any factor node from a factor graph leaves the adjacent variable nodes independent with respect to the resulting distribution [49]. This translates into the independence of the incoming messages to any factor node. We refer to this condition as the *replica symmetric assumption*. The replica symmetric assumption may not hold when the factor graph contains short loops or when the variables are correlated over large distances (the notion of distance between two variable nodes can be given by the number of factor nodes along a path connecting them). For graphs that are locally tree-like, long-distance correlations are responsible for the breakdown of BP. These long-range correlations often signal a phase transition, where solutions cluster in a well-separated region of the space of solutions. This phenomenon is referred to as one-step replica symmetry breaking (1RSB). We describe this in more detail in Section B.

## A.1 Supplementary results for $m_{\text{sample}}^*$ with $d = 6$

While the results for  $m_{\text{sample}}^*$  for  $d = 3, 4, 5$  are available in [7, 8], the results for  $d = 6$  were not available. Hence, we computed them as the intersection between the entropy for the  $c = 2$  cycles and the trajectories reaching the homogeneous  $+1$  attractor for  $p = 1, 2, 3$ . In Figure 6 we show that in order to find the

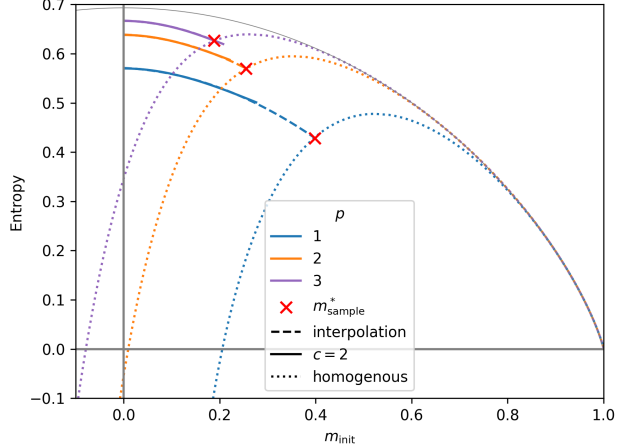


Figure 6: RS entropy for the attractor that is a  $c = 2$  cycle and the homogeneous  $+1$  point attractor, for  $d = 6$  with the always-stay tie-breaking rule and  $p = 1, 2, 3$ . The transition where the dominating entropy changes is marked with a red point,  $m_{\text{sample}}^*$ . Where the line is dashed we extrapolated the entropy for  $c = 2$  using a quadratic function.

intersection, we had to extrapolate the  $c = 2$  entropy using a quadratic fit. This is because the equations becomes unstable as one reaches the fixed point of the homogeneous  $+1$  attractor. This leads us to the values for  $m_{\text{sample}}^*$  reported in Table 2.

## B One-step Replica Symmetry Breaking

In this section, we provide an overview-level treatment of the 1RSB mechanism, with an emphasis on the BDCM formalism. We interpret the setting of Section 4 as an example of a dynamical constraint satisfaction problem. Accordingly, we refer to initializations with a given  $m_{\text{init}}$  that evolve to full consensus under majority dynamics on sparse random graphs as *solutions* of this problem. The constraints are: adherence to the dynamical rule, the trajectory being a valid  $(p, c)$  backtracking attractor, a fixed trajectory value in the attractor, and the prescribed initial magnetization.

### B.1 Definition and intuition of 1RSB

We introduce the 1RSB through the lens of the clustering phenomenon appearing in the space of possible trajectories. To define clusters, we introduce a metric on the solution space. For any two solutions  $\mathbf{s}_1, \mathbf{s}_2 \in S^n$ , the *Hamming distance*  $d_H(\mathbf{s}_1, \mathbf{s}_2)$  is defined as the number of node values in  $\mathbf{s}_2$  that differ from  $\mathbf{s}_1$ . We say that two solutions  $\mathbf{s}_1, \mathbf{s}_2$  are *finitely close*, when, for large  $n$ , we have  $d_H(\mathbf{s}_1, \mathbf{s}_2) = O(1)$ . In other words, the two solutions differ at a finite (i.e. non-growing) number of variables. We define a *cluster*  $C \subset S^n$  as a maximal set of solutions, where for any two solutions  $\mathbf{s}_A, \mathbf{s}_B \in C$ , we have a path of *solutions*  $\mathcal{S} = \{\mathbf{s}_1, \mathbf{s}_2, \dots\} \subset C$  connecting them, in such a way that any two consecutive solutions on the path  $\mathbf{s}_A, \mathbf{s}_1, \mathbf{s}_2, \dots, \mathbf{s}_N, \mathbf{s}_B$  are finitely close in the Hamming distance.

In the replica symmetric (RS) phase, the BDCM is exact and the solutions form one thermodynamically relevant cluster (we describe thermodynamical relevance below). More generally, BDCM remains exact when removing any factor node from a factor graph leaves the adjacent variable nodes independent with respect to the resulting distribution [49], or equivalently, when the incoming messages to any factor node are independent. This is straightforwardly the case for a tree. However, since there are only long cycles ( $\sim \log(n)$  or longer) through a typical node in large random graphs *and* no long-range correlations, the BDCM is still asymptotically exact [49, 42]. In other words, settings with graphs that contain long cycles on which the message correlations decay quickly are RS. An example of this are *weakly interacting* models such as CSPs with a low number of constraints compared to the number of variables (the corresponding factor graph is sparse:  $|\partial A_i| \ll n$ ) and/or large temperatures (small values of the Lagrange parameters) [12]. When there is

a global symmetry (e.g.,  $\mathbb{Z}_2$  symmetry in the Ising model), there is a finite set of thermodynamically relevant clusters, but we still describe this situation as RS.

When long-range correlations are present, solutions might be gathered in different clusters. Intuitively, when we have a large density of constraints, transforming one solution into another cannot *always* be done in finitely many variable changes. Few local changes can immediately propagate to an extensive distance in order to still satisfy all the constraints. When there is no path of incremental changes through solutions to other solutions (as defined above), we have clusters. The replica symmetry is broken. When the solution space is accurately described by the decomposition of the RS cluster into smaller clusters (with no further internal structure), we say that there is a *one-step replica symmetry breaking* [41]. The 1RSB phase is associated with two scenarios, dynamical and static 1RSB.

In the dynamical one-step replica symmetry breaking (d1RSB) scenario, we have exponentially many thermodynamically relevant clusters, each associated with a BP fixed point. The RS Bethe free entropy density is still exact. If one adds constraints or changes the Lagrange parameters, the number of relevant clusters can become sub-exponential: we have static one-step replica symmetry breaking (s1RSB). Long-range correlations are stronger than in the d1RSB phase, and BP procedures lead to an incorrect estimate of the free entropy density [43]. However, within the clusters BP is still correct – this is the assumption that holds both in dynamical and static 1RSB. Furthermore, we still assume the one-to-one correspondence between clusters and BP fixed points.

As the number of constraints increases further, the clusters vanish and the problem becomes unsatisfiable (UNSAT).

## B.2 1RSB equations

First, we repeat for convenience the definitions of the main 1RSB quantities described in Section 3. We introduce a Boltzmann distribution over the clusters associated with fixed points  $\tilde{\chi} = \{\chi^{i \rightarrow j}, \chi^{j \rightarrow i}\}_{(ij) \in E}$  with  $\chi^{i \rightarrow j} = \{\chi_{\underline{x}_i, \underline{x}_j}^{i \rightarrow j}\}_{(\underline{x}_i, \underline{x}_j) \in S^{2(p+c)}}$ :

$$P_{1\text{RSB}}(\tilde{\chi}) = \frac{1}{Z_{1\text{RSB}}} e^{nr\Phi_{\text{int}}(\tilde{\chi})}. \quad (50)$$

$r$  is the *Parisi parameter*,  $Z_{1\text{RSB}}$  is the normalization and  $\Phi_{\text{int}}(\tilde{\chi})$  is the Bethe free entropy density computed from the fixed point  $\tilde{\chi}$  according to equation (9). We call it the *internal* free entropy density as it is the free entropy density of a cluster. We also define the *replicated* free entropy density:

$$\Psi(r) = \frac{\log(Z_{1\text{RSB}}(r))}{n}. \quad (51)$$

Furthermore, the exponentially leading number of clusters with  $\Phi_{\text{int}}$  is given by the *complexity*  $\Sigma(\Phi_{\text{int}})$ :

$$\Sigma(\Phi_{\text{int}}) = \frac{\log \mathcal{N}(\Phi_{\text{int}})}{n}, \quad (52)$$

where  $\mathcal{N}(\Phi_{\text{int}})$  is the total number of clusters with internal free entropy density  $\Phi_{\text{int}}$ . Using the complexity, we express the partition function  $Z_{1\text{RSB}}$  through an integral over all possible internal free entropy densities as

$$Z_{1\text{RSB}} = e^{n\Psi(r)} = \sum_{\tilde{\chi}} e^{nr\Phi_{\text{int}}(\tilde{\chi})} = \sum_{\Phi_{\text{int}}} \mathcal{N}(\Phi_{\text{int}}) e^{nr\Phi_{\text{int}}(\tilde{\chi})} \simeq \int d\Phi_{\text{int}} e^{n(r\Phi_{\text{int}} + \Sigma(\Phi_{\text{int}}))}. \quad (53)$$

Next, we proceed in a similar way as in Section 3. Utilizing the saddle-point method with  $n \rightarrow \infty$ , equation (53) becomes

$$\Psi(r) = r\hat{\Phi}_{\text{int}} + \Sigma(\hat{\Phi}_{\text{int}}), \quad (54)$$

where  $\hat{\Phi}_{\text{int}}$  extremizes  $\Psi(r)$ . Moreover, we have

$$\left. \frac{\partial \Sigma(\Phi_{\text{int}})}{\partial \Phi_{\text{int}}} \right|_{\Phi_{\text{int}}=\hat{\Phi}_{\text{int}}} = -r. \quad (55)$$

If we could sample solutions uniformly at random, we would see with probability approaching 1 as  $n \rightarrow \infty$  only the solutions from clusters whose  $\Phi_{\text{int}}$  maximizes the measure (12). In other words, this  $\Phi_{\text{int}}$  maximizes the *total free entropy density*

$$\Psi_{\text{tot}} = \Phi_{\text{int}} + \Sigma(\Phi_{\text{int}}), \quad (56)$$

which gives the total (unbiased by  $r$ ) number of solutions. Typical solutions are those that jointly maximize  $\Phi_{\text{int}}$  (size) and  $\Sigma$  (number of clusters). The total free entropy density is maximized (with respect to  $\Phi_{\text{int}}$ ) by  $\hat{\Phi}_{\text{int}}$  for  $r = 1$ , since  $\Psi_{\text{tot}} = \Psi(1)$  and  $\hat{\Phi}_{\text{int}}$  is the maximizer of  $\Psi(r)$  for all  $r$ .

If the complexity for  $r = 1$  is positive, we are in the d1RSB. We have *exponentially* many *thermodynamically relevant* clusters, i.e. their  $\Phi_{\text{int}} = \hat{\Phi}_{\text{int}}$ . A negative complexity is not physical (we assume that solutions exist; hence there needs to be at least one cluster). Thus, when the complexity is negative for  $r = 1$ , we need to maximize the total free entropy with the constraint  $\Sigma \geq 0$ . We refer to  $\Phi_{\text{int}}$  satisfying this as  $\Phi_s$ , and we are in the s1RSB phase. That said, the constraint  $\Sigma \geq 0$  cannot be enforced locally and is not part of the BDCM equations. Hence,  $\Phi_s$  is obtained by computing the complexity as a function of  $\Phi_{\text{int}}$ , and  $\Phi_s$  is equal to  $\Phi_{\text{int}}$  for which  $\Sigma(\Phi_{\text{int}}) = 0$ . We can get  $\Phi_{\text{int}}$  for a given  $r$  as

$$\Phi_{\text{int}} = \frac{\partial \Psi(r)}{\partial r}, \quad (57)$$

as seen from the 1RSB probability distribution (12) and the definition of  $\Psi(r)$  (13) (we assume self-averaging in the thermodynamic limit). Thus, we can get the complexity from (15) and by varying  $r \in [0, 1]$ , we can find  $\Phi_s$ .

There is, however, a familiar obstacle: obtaining  $\Psi$  requires computing  $Z_{1\text{RSB}}$ , which is generally intractable. To address this, we devise one more BP procedure to estimate it. Again, we suppose that the original graph  $G$  is a tree and we can construct the factor graph as in section A. We then rewrite the BDCM update rule (8) as

$$\chi_{\underline{x}_i, \underline{x}_j}^{i \rightarrow j} = \frac{1}{Z^{i \rightarrow j}} a(\underline{x}_i, \underline{x}_j) \sum_{\{\underline{x}_{\partial i \setminus j}\}} \mathcal{A}_i(\underline{x}_i, \underline{x}_{\partial i}) \prod_{k \in \partial i \setminus j} \chi_{\underline{x}_k, \underline{x}_i}^{k \rightarrow i} = \mathcal{F}(\{\chi_{\underline{x}_k, \underline{x}_i}^{k \rightarrow i}\}_{k \in \partial i \setminus j}). \quad (58)$$

To lighten the notation, we write the message  $\chi_{\underline{x}_i, \underline{x}_j}^{i \rightarrow j}$  without the subscript, which refers to all components of the message. Hence, if (58) is true for all combinations of variable node trajectories  $(\underline{x}_i, \underline{x}_j) \in S^{2(p+c)}$ , we have

$$\chi^{i \rightarrow j} = \mathcal{F}(\{\chi^{k \rightarrow i}\}_{k \in \partial i \setminus j}). \quad (59)$$

We refer to all the messages on the graph  $\{\chi^{i \rightarrow j}, \chi^{j \rightarrow i}\}_{(ij) \in E}$  simply as  $\chi$ . When all messages satisfy (59), i.e. when we have a BP fixed point, we denote  $\chi$  as  $\tilde{\chi}$  as before.

In 1RSB we suppose that the measure  $P$  (2) can be approximated by the messages inside the clusters. Thus, we obtain the internal free entropy density  $\Phi_{\text{int}}$  as the Bethe free entropy density (9). Consequently, we express the 1RSB partition function as

$$\begin{aligned} Z_{1\text{RSB}} &= \sum_{\tilde{\chi}} e^{nr\Phi_{\text{int}}(\tilde{\chi})} = \int d\chi e^{r(\sum_i \log Z^i - \sum_{(ij)} \log Z^{ij})} \prod_i \prod_{j \in \partial i} \delta(\chi^{i \rightarrow j} - \mathcal{F}(\{\chi^{k \rightarrow i}\}_{k \in \partial i \setminus j})) \\ &= \int d\chi \prod_i (Z^i)^r \prod_{(ij)} (Z^{ij})^{-r} \prod_i \prod_{j \in \partial i} \delta(\chi^{i \rightarrow j} - \mathcal{F}(\{\chi^{k \rightarrow i}\}_{k \in \partial i \setminus j})), \end{aligned} \quad (60)$$

where the integral goes over all possible message values with the condition that the messages are normalized:  $\sum_{\{\underline{x}_i, \underline{x}_j\}} \chi_{\underline{x}_i, \underline{x}_j}^{i \rightarrow j} = 1$ .  $\delta()$  is the Dirac delta. We can interpret equation (60) as the partition function of the probability distribution

$$\tilde{P}(\chi) = \frac{1}{\tilde{Z}} \prod_i (Z^i)^r \prod_{(ij)} (Z^{ij})^{-r} \prod_i \prod_{j \in \partial i} \delta(\chi^{i \rightarrow j} - \mathcal{F}(\{\chi^{k \rightarrow i}\}_{k \in \partial i \setminus j})). \quad (61)$$

When the graph  $G$  is a tree, we have:  $|V| = |E| + 1$ . Hence, we can associate every edge with one unique node, except for one edge, which is associated with two nodes. We then formulate (61) as

$$\tilde{P}(\chi) = \frac{1}{\tilde{Z}} \prod_{(ij)} \left( \frac{Z^i}{Z^{ij}} \right)^r \delta(\chi^{i \rightarrow j} - \mathcal{F}(\{\chi^{k \rightarrow i}\}_{k \in \partial i \setminus j})) \delta(\chi^{j \rightarrow i} - \mathcal{F}(\{\chi^{k \rightarrow j}\}_{k \in \partial j \setminus i})). \quad (62)$$

We note that  $Z^i/Z^{ij} = Z^{i \rightarrow j}$  as shown in (47). We construct a graphical representation of (62) in the form of a factor graph, similarly as in section A. This time, for every edge of the original graph, we have pairs of messages  $(\chi^{i \rightarrow j}, \chi^{j \rightarrow i})$  as variable nodes. In our notation, we have neglected the dependence of the  $Z^i$ s and  $Z^{ij}$ s on the messages. Note that  $Z^{ij}$  is a function of only  $\chi^{i \rightarrow j}$  and  $\chi^{j \rightarrow i}$ , as seen in (11). Thus, the corresponding factor nodes in the factor graph are attached only to the variable nodes  $(\chi^{i \rightarrow j}, \chi^{j \rightarrow i})$ .  $Z^i$ s (10) are functions of  $\{\chi^{k \rightarrow i}\}_{k \in \partial i}$ . Hence, they are parts of the factor nodes  $\delta_{i,j}$  that represent the delta functions in (62):

$$\delta_{i,j} = (Z^i)^r \delta(\chi^{i \rightarrow j} - \mathcal{F}(\{\chi^{k \rightarrow i}\}_{k \in \partial i \setminus j})) . \quad (63)$$

In place of a node  $i$  in the original graph, we now have a factor node  $\delta_{i,j}$  (and  $\delta_{j,i}$  for  $j$ ). The structure of the factor graph is the same as before (see Figure 7).

We again introduce partial partition functions on the factor graph, beliefs  $P^{i \rightarrow j}$  conditioned on the message values  $\chi^{i \rightarrow j}$  and obtain the BP equations for them:

$$\begin{aligned} P^{i \rightarrow j}(\chi^{i \rightarrow j}) &= \frac{1}{Z^{i \rightarrow j}} \int \{d\chi^{k \rightarrow i}\}_{k \in \partial i \setminus j} \left( \frac{Z^i}{Z^{ij}} \right)^r \delta(\chi^{i \rightarrow j} - \mathcal{F}(\{\chi^{k \rightarrow i}\}_{k \in \partial i \setminus j})) \times \\ &\quad \times \prod_{k \in \partial i \setminus j} P^{k \rightarrow i}(\chi^{k \rightarrow i}), \end{aligned} \quad (64)$$

where  $Z^{i \rightarrow j}$  is the normalization. We lighten the notation by not explicitly denoting the dependence on the messages and by merging the differentials with the beliefs  $P^{k \rightarrow i}$ :

$$\{d\chi^{k \rightarrow i}\}_{k \in \partial i \setminus j} \prod_{k \in \partial i \setminus j} P^{k \rightarrow i}(\chi^{k \rightarrow i}) = \prod_{k \in \partial i \setminus j} dP^{k \rightarrow i}. \quad (65)$$

To compute the replicated free entropy density, we follow the same procedure used to obtain (9) (since the

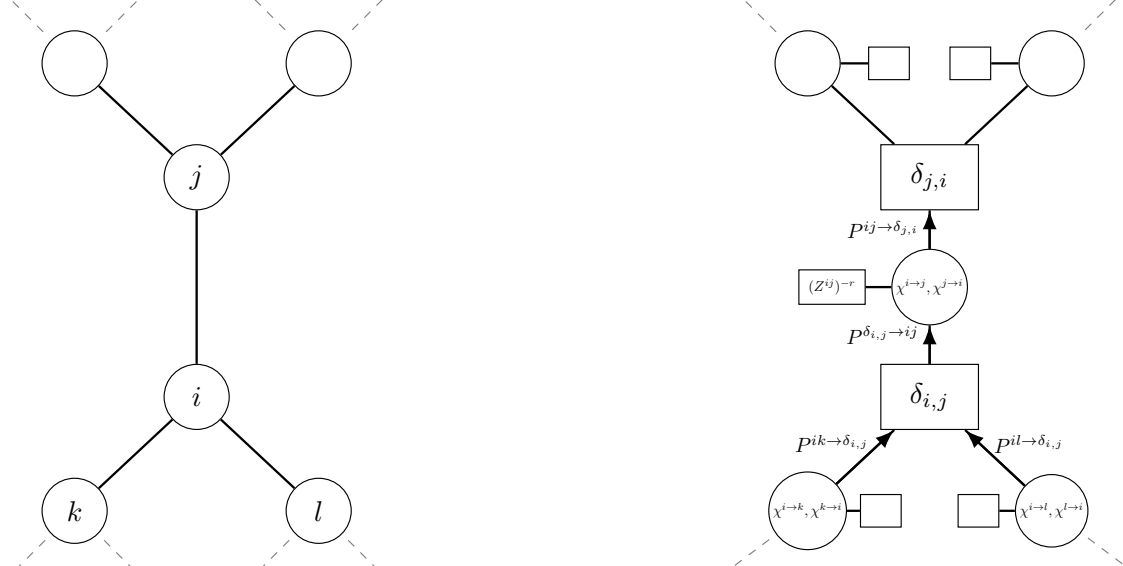


Figure 7: Factor graph construction for the 1RSB probability distribution (62). (Left.) Part of the original tree graph  $G$ . (Right.) Factor graph with message pairs as variable nodes, and with  $(Z^{ij})^{-r}$ s (11) and  $\delta_{i,j}$ s (63) as factor nodes. BP update for the beliefs  $P^{ij} \rightarrow \delta_{j,i}$  is given by  $(Z^{ij})^{-r} P^{\delta_{i,j} \rightarrow ij}$ , hence we can write self-consistent BP equations only for the beliefs going into the factor nodes as (64). In the main text we shorten the notation from  $P^{ij} \rightarrow \delta_{j,i}$  to  $P^{i \rightarrow j}$ .

factor graph has the same structure in both cases):

$$\Psi(r) = \frac{1}{n} \left( \sum_{i \in V} \log \mathcal{Z}^i - \sum_{(ij) \in E} \log \mathcal{Z}^{ij} \right) \quad (66)$$

where

$$\mathcal{Z}^i = \int \prod_{k \in \partial i} dP^{k \rightarrow i} (Z^i)^r, \quad (67)$$

and

$$\mathcal{Z}^{ij} = \int dP^{i \rightarrow j} dP^{j \rightarrow i} (Z^{ij})^r. \quad (68)$$

On RRGs, we can again use the fact that every node has the same number of neighbors (see Section 4.1) to simplify the equations and obtain the average values over the ensemble of RRGs. The 1RSB equations then read

$$P^{\rightarrow}(\chi^{\rightarrow}) = \frac{1}{\mathcal{Z}^{\rightarrow}} \int \prod_{k=1, \dots, d-1} dP^{\rightarrow}(\chi_k^{\rightarrow}) \left( \frac{Z^{\text{fac}}}{Z^{\text{var}}} \right)^r \delta(\chi^{\rightarrow} - \mathcal{F}(\{\chi_k^{\rightarrow}\}_{k=1, \dots, d-1})), \quad (69)$$

where  $Z^{\text{fac}}$  and  $Z^{\text{var}}$  are defined in eqs. (21) and (22).  $\Psi(r)$  is given by

$$\Psi(r) = \log \mathcal{Z}^{\text{fac}} - \frac{d}{2} \log \mathcal{Z}^{\text{var}}, \quad (70)$$

where

$$\mathcal{Z}^{\text{fac}} = \int \prod_{k=1, \dots, d-1} dP^{\rightarrow}(\chi_k^{\rightarrow}) (Z^{\text{fac}})^r, \quad (71)$$

and

$$\mathcal{Z}^{\text{var}} = \int dP^{\rightarrow}(\chi_1^{\rightarrow}) dP^{\rightarrow}(\chi_2^{\rightarrow}) (Z^{\text{var}})^r. \quad (72)$$

Again we did not note the dependence on the messages. The internal free entropy and complexity can again be obtained from eqs (57) and the complexity from (54).

### B.3 Population Dynamics

Here we present a widely used procedure for solving the 1RSB equations (64). Note that the population dynamics numerical scheme can be used for any distributional equations of this type, including RS BP. In the context of the cavity method, it was developed in [50]. The main idea is to represent the probability distribution by  $N$  (ideally) i.i.d. samples from it. These  $N$  samples are called a *population*. Then, we update the population so that it converges to the fixed point of the 1RSB equations. In the 1RSB eqs. (69), we have a continuous probability distribution (represented by a population) over messages, which are themselves a discrete probability distribution over variable node trajectories. We describe the variant of population dynamics that we use below, and other treatments are available in e.g. [67, 41, 49].

1. Initialize a set of  $N$  messages (the population). The messages are initialized uniformly at random on *hard-fields*: messages are set to 1 for some trajectories combination  $\underline{x}_i, \underline{x}_j$  and 0 for all others. The hard-fields initialization is justified by the reconstruction on trees setting [48] and further commented on in [41]. If the population is instead initialized from a random uniform distribution, it typically converges to the RS fixed point, resulting in a delta-function distribution centered at the RS fixed-point value.
2. Choose uniformly at random  $M = \varepsilon N$  messages from the population. We call this  $M$  messages a *subpopulation*. The  $\varepsilon$  represents damping and makes the procedure numerically more stable.
3. Update each message in the subpopulation using the BDCM update rule (59). The BDCM update is computed by sampling  $d-1$  (in the case of a RRG) messages uniformly at random from the *entire* population.
4. Compute the normalization  $Z^{i \rightarrow j} = Z^i / Z^{ij}$  (47) for each message of the updated subpopulation. Number the messages of the subpopulation and their normalizations with  $k = 1, 2, \dots, M$ . We call  $Z_k$  the  $Z^{i \rightarrow j}$  normalization of the  $k$ th message.

5. Create a new subpopulation of  $M$  messages sampled from the updated subpopulation from steps 3 and 4. Sample the messages into the new subpopulation according to the distribution  $P(k) = Z_k^r / \sum_{i=1}^M Z_i^r$ . Replace the  $M$  originally sampled messages with this new subpopulation.
6. Repeat from step 2 or stop if the population converged.

The probability distribution over messages is then obtained from the normalized histogram of the population: the number of samples with a given message value is proportional to the probability of that message value estimated by the 1RSB fixed point. Once the histogram ceases to change significantly, we say that the population converged. Observables can then be computed from the converged population, as we discuss below.

In this process, we approximate the distributions by the populations and we also approximate the 1RSB update (64). Step 3 ensures that all messages satisfy the BDCM update, as mandated by the delta function in (64). By doing steps 4 and 5 we weight the messages with  $(Z^i/Z^{ij})^r$ . Thus, the integral is effectively replaced by the representation of the distributions by populations. Indeed, the  $\prod_{k \in \partial_i \setminus j} dP^{k \rightarrow i}$  is approximated by the random choice of update messages in 3., with the additional fact that each message value can appear multiple times. Consequently, the messages sampled in step 3 are selected with probabilities proportional to their 1RSB beliefs.

**Observables.** The replicated free entropy density (70) is estimated from the converged population. We take  $\sim N$  messages from the population and approximate the integrals (71) and (72) with them. For better precision, this is repeated several times (possibly for multiple iterations of the population dynamics, where there may be an interval between the iterations used for computation), and then the average is taken. In general, any observables that depend on messages  $\{\chi^\rightarrow\}$  or on 1RSB beliefs  $\{P^\rightarrow\}$  can be estimated this way.

In population dynamics, the d1RSB phase is recognized when the population for  $r = 1$  converges to a different than RS fixed point, i.e. the solution to 1RSB equations (69) is not trivial. Moreover, both the internal free entropy density (which is the same as the RS estimation) and complexity are positive.

In the s1RSB phase, the free entropy density is different from that estimated by the RS BDCM (9). The complexity is null and  $\Phi_s$  is determined by the procedure described in Section B.2 and illustrated in Figure 3.

## B.4 On the s1RSB results

Table 1 from the main text presents the s1RSB results for  $p = 1$ . To correctly determine the s1RSB phase, we need to explore a range of Parisi parameter values as described in Section B.2. Figure 3 shows the complexity as a function of the initial magnetization. The s1RSB initial magnetization is obtained when the complexity becomes positive. Obtaining the  $m_{\text{init}}$  values that mark the s1RSB phase in the cases of some  $p = 2$  and  $p = 3$  requires large arrays of messages to model the distributions. We were not able to get sufficiently stable populations to estimate the s1RSB initial magnetization in these cases.

In Figure 8 and 9 we show the s1RSB results for  $p = 2, 3$  that we were able to obtain. Due to the increasing instability in the equations, it proved very difficult to compute them numerically for increasing values of  $d$  and  $p$ , which resulted in only very unreliable results on the s1RSB transition for  $p = 3$  in Figure 9.

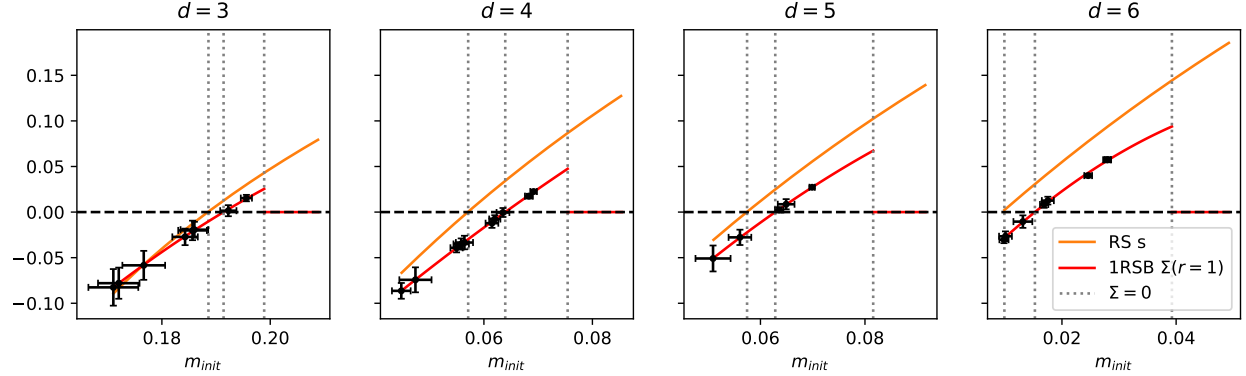


Figure 8: Thresholds of  $m_{RS}^*$ ,  $m_{sRSB}^*$  and  $m_{dRSB}^*$  (from left to right) for  $p = 2$  and different values of  $d$ . Each black point represents the complexity  $\Sigma$  obtained from the 1RSB equations for a single  $\lambda$ , and the error on the sample mean is indicated by error bars in  $x$  and  $y$  over 10 differently initialized runs of the population dynamics. For each run, the complexity is estimated as an average of complexity obtained from the last 100 iterations in the process. The red curve is a quadratic fit of this data, which ends at  $m_{dRSB}^*$  from Table 2.

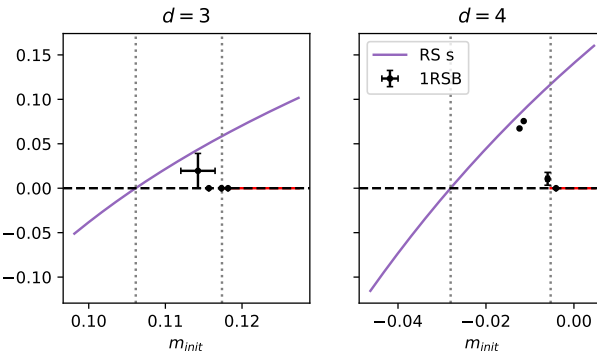


Figure 9: Thresholds of  $m_{RS}^*$  and  $m_{dRSB}^*$  (from left to right) for  $p = 3$  and  $d = 3, 4$ . Each black point represents the complexity  $\Sigma$  obtained from the 1RSB equations for a single  $\lambda$ , and the error on the sample mean is indicated by error bars in  $x$  and  $y$  over 2 samples, if no error bars are present, only one sample was generated.

## B.5 Numerical evidence of freezing for $p = 1, d = 4$

To provide numerical evidence for the predicted frozen phase, we analyze the converged message population to identify variables with deterministically fixed values. We focus on the  $p = 1, d = 4$  case, which offers greater numerical precision compared to systems with larger  $p$ . For these parameters, the problem is equivalent to a CSP where each  $-1$  node must have strictly more than two  $+1$  neighbors, and each  $+1$  node must have at least two  $+1$  neighbors. This equivalence permits more extensive simulations. We use the code provided in [41], which implements the population dynamics for this CSP. We performed simulations with a population of  $10^7$  messages, iterated  $10^4$  times with a damping factor  $\varepsilon = 0.2$ .

Our results show the emergence of a frozen phase at an initial magnetization  $m_{init} = 0.258(2)$ . The number in parentheses is the last common digit for simulations just before and after the onset of the rigid phase. This result is consistent with the one obtained from our implementation of the population dynamics. Within this phase, we find that approximately 60% of the variables are frozen. This value is obtained by the fraction of messages in the converged population that assign a probability  $> 0.99$  to a given node. Although freezing requires this probability to be exactly 1, the use of a threshold is necessitated by the finite precision of our numerical method, which is limited by population size, iteration count, and floating-point arithmetic.

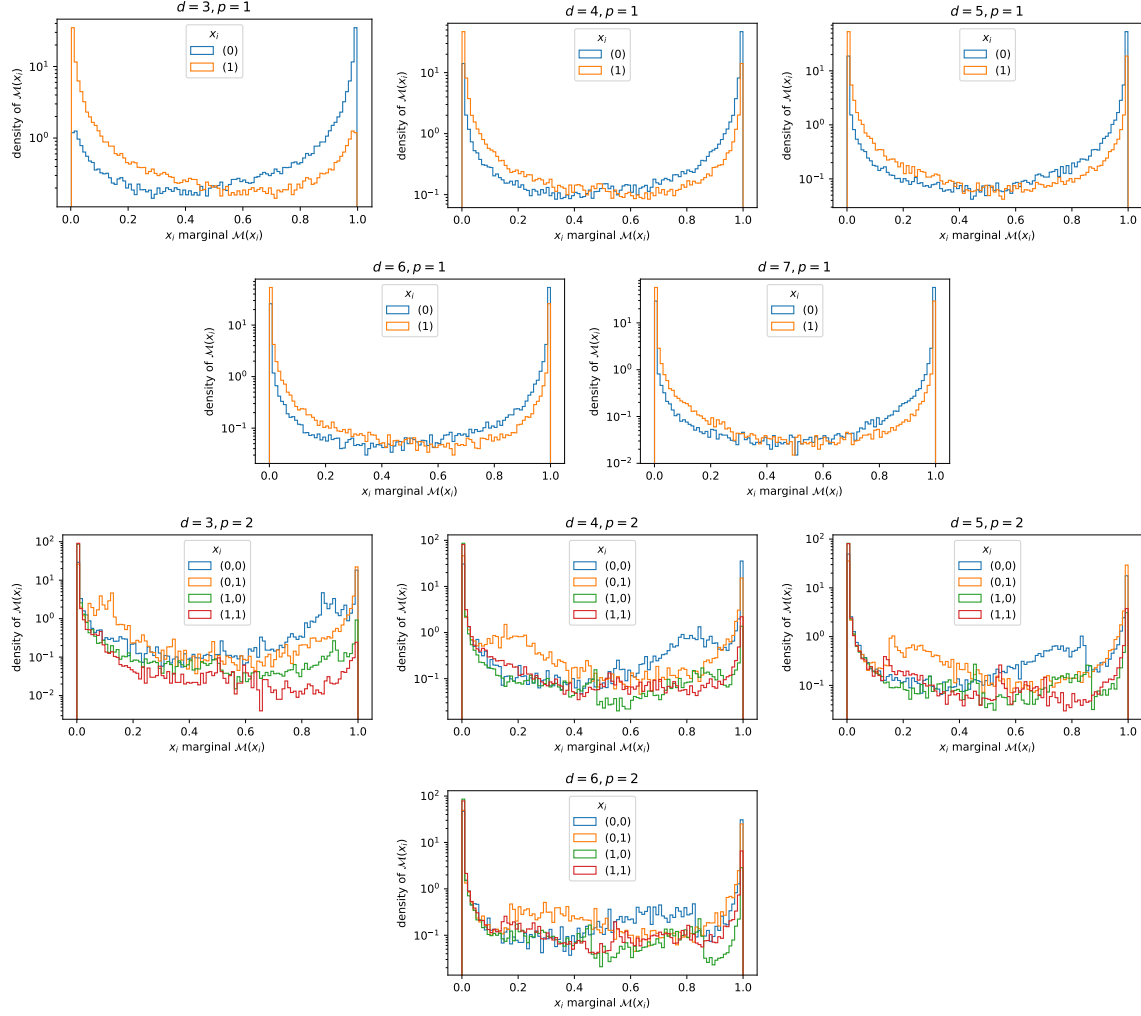


Figure 10: For each combination of  $d, p$  we select the 1RSB fixed point which has the largest  $m_{\text{init}}$  with a complexity  $\Sigma > 0$ , and thereby has 1RSB behavior in Table 3. For the associated equilibrated population of 100 000 messages, we show the density over the values of the marginals of the outgoing node, i.e. the density over  $\mathcal{M}(\underline{x}_i) = \sum_{\{\underline{x}_j\}} \chi_{\underline{x}_i, \underline{x}_j}$ .

Consequently, our analysis cannot definitively distinguish between variables that are genuinely frozen and those that are “almost frozen”. A similar situation arises in certain settings for the coloring problem of random graphs, and is discussed more in depth in [68]. Resolving this distinction remains an open question for future work.

For larger values of  $p$ , the use of smaller populations makes the numerical detection of this frozen phase even more unclear. Figure 10 shows the marginal probability histograms for  $p = 1, 2$  and various  $d$  in the d1RSB phase. The histograms peak at 0 and 1, as expected for frozen variables. However, as discussed above, this is not enough to ensure the presence of frozen variables.

## C History Passing

### C.1 Derivation of the marginals equation in HPR

Here we derive the relation for the marginals (25). The marginal probability distribution is defined as

$$\mu_{x_i^1=s}^i = \sum_{\{\underline{x}\}} \mathbb{1} [x_i^1 = s] P(\underline{x}). \quad (73)$$

We rewrite it similarly as the partition function  $Z$  in (31) and obtain

$$\mu_{x_i^1=s}^i = \frac{1}{Z} \sum_{\{\underline{x}_i, \underline{x}_{\partial i}\}} \mathbb{1} [x_i^1 = s] \mathcal{A}_i(\underline{x}_i, \underline{x}_{\partial i}) \prod_{ij \in \partial A_i} V_{\underline{x}_i, \underline{x}_j}^{ij \rightarrow A_i}. \quad (74)$$

Furthermore, multiplying (74) by unity, we have

$$\begin{aligned} \mu_{x_i^1=s}^i &= \frac{1}{Z} \sum_{\{\underline{x}_i, \underline{x}_{\partial i}\}} \mathbb{1} [x_i^1 = s] \mathcal{A}_i(\underline{x}_i, \underline{x}_{\partial i}) \prod_{ij \in \partial A_i} V_{\underline{x}_i, \underline{x}_j}^{ij \rightarrow A_i} \cdot \frac{\prod_{ij \in \partial A_i} \sum_{\{\underline{x}'_i, \underline{x}'_j\}} V_{\underline{x}'_j, \underline{x}'_i}^{ij \rightarrow A_i}}{\prod_{ij \in \partial A_i} \sum_{\{\underline{x}'_i, \underline{x}'_j\}} V_{\underline{x}'_j, \underline{x}'_i}^{ij \rightarrow A_i}} \\ &\stackrel{(39)}{=} \frac{1}{\tilde{Z}_c} \sum_{\{\underline{x}_i, \underline{x}_{\partial i}\}} \mathbb{1} [x_i^1 = s] \mathcal{A}_i(\underline{x}_i, \underline{x}_{\partial i}) \prod_{ij \in \partial A_i} \chi_{\underline{x}_j, \underline{x}_i}^{j \rightarrow i}, \end{aligned} \quad (75)$$

where we have defined  $1/\tilde{Z}_c = \prod_{ij \in \partial A_i} \sum_{\{\underline{x}'_i, \underline{x}'_j\}} V_{\underline{x}'_j, \underline{x}'_i}^{ij \rightarrow A_i} / Z$ . In (75), with  $ij \in A_i \Leftrightarrow j \in \partial i$ , we recognize the BDCM fixed point equation (8)

$$\begin{aligned} \mu_{x_i^1=s}^i &= \frac{1}{\tilde{Z}_c} \sum_{\{\underline{x}_i, \underline{x}_j\}} \mathbb{1} [x_i^1 = s] \frac{Z^{i \rightarrow j}}{a(\underline{x}_i, \underline{x}_j)} \left( \frac{a(\underline{x}_i, \underline{x}_j)}{Z^{i \rightarrow j}} \sum_{\{\underline{x}_{\partial i \setminus j}\}} \mathcal{A}_i(\underline{x}_i, \underline{x}_{\partial i}) \prod_{k \in \partial i \setminus j} \chi_{\underline{x}_k, \underline{x}_i}^{k \rightarrow i} \right) \chi_{\underline{x}_j, \underline{x}_i}^{j \rightarrow i} = \\ &= \frac{Z^{i \rightarrow j}}{\tilde{Z}_c} \sum_{\{\underline{x}_i, \underline{x}_j\}} \frac{\mathbb{1} [x_i^1 = s]}{a(\underline{x}_i, \underline{x}_j)} \chi_{\underline{x}_i, \underline{x}_j}^{i \rightarrow j} \chi_{\underline{x}_j, \underline{x}_i}^{j \rightarrow i} = Z_{x_i^1=s}^{ij}, \end{aligned} \quad (76)$$

and we get (26) with  $Z_c = Z^{i \rightarrow j} / \tilde{Z}_c$ . Note that we can pick *any* neighboring node  $j \in \partial i$  and use the BDCM equation in (76). This is the case for the *converged* BDCM messages on the tree factor graphs (or more generally, in settings where the RS assumption holds).

However, in the history passing reinforcement (HPR), we have biases that break the symmetry. By choosing  $j \in \partial i$  we get the message pair  $\chi_{\underline{x}_i, \underline{x}_j}^{i \rightarrow j} \chi_{\underline{x}_j, \underline{x}_i}^{j \rightarrow i}$ , where a particular, edge dependent, set of biases is present through the biased message updates (23). Furthermore, in the biased BDCM update equation (23), we have a nonlinear relation between the messages and marginals constructed from them, where the message update depends on the marginals via the (changing) biases. Hence, during the HPR run, the messages do not have to converge to the fixed point values because these values change with the values of changing biases (these are in fact the settings in which the HPR is effective), as can be seen in Figure 11 (left). Thus,  $Z_{x_i^1=s}^{ij}$  for different neighbors  $j$  can differ. To get the marginal estimates from the messages, we collect all the available information and combine it into one edge-independent marginal estimate. We arrive at the following product over neighboring edges

$$\mu_{x_i^1=s}^i = \frac{1}{Z_\mu} \prod_{j \in \partial i} Z_{x_i^1=s}^{ij}, \quad (77)$$

which is (25). This is in fact sufficient, since for the bias update (24) we ultimately only need to compare the current marginals for node  $i$  starting with  $\pm 1$ .

### C.2 Time Dynamics

**Convergence.** Figure 11 shows supplementary results about the HPR algorithm, completing the discussion in section 5. The maximum message change  $\Delta$  is defined as

$$\Delta = \max_{i, j, \underline{x}_i, \underline{x}_j} \left| \chi_{\underline{x}_i, \underline{x}_j}^{i \rightarrow j} \text{(after)} - \chi_{\underline{x}_i, \underline{x}_j}^{i \rightarrow j} \text{(before)} \right|. \quad (78)$$

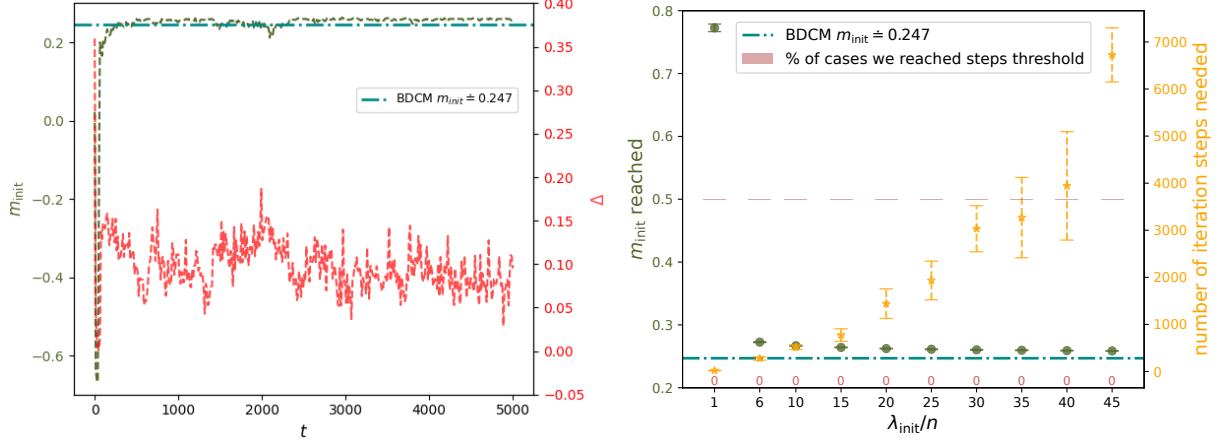


Figure 11: (Left) Evolution of biases as reflected in the initial magnetization  $m(\mathbf{x}^{\text{sol}})$  and convergence of messages measured by maximum message change  $\Delta$  in the HPR algorithm. We see that the  $m(\mathbf{x}^{\text{sol}})$  can quickly approach the final value returned by the algorithm, but the messages (hence, also the biases) continue to change for some time, before finding the true solution. Parameters used:  $n = 1000$ ,  $d = 4$ ,  $p = 1 = c$ ,  $\pi = 0.3$ ,  $\gamma = 0.1$ ,  $\varepsilon = 0.4$ ,  $\lambda_{\text{init}} = 25$ . (Right) Obtained initial magnetization  $m_{\text{init}}$  and number of iterations needed (we stop the HPR algorithm when we reach the solution for the first time) as function of the Lagrange parameter  $\lambda_{\text{init}}$  for  $n = 10000$ ,  $d = 4$ ,  $p = 1 = c$ ,  $\pi = 0.3$ ,  $\gamma = 0.1$  and  $\varepsilon = 0.4$ . Error bars depict the standard deviation, the number of repetitions for each  $\lambda_{\text{init}}$  was 10, except for  $\lambda_{\text{init}} = 40, 45$  where it was 5 and 2 respectively. The reached minimal magnetizations plateau before reaching the  $m_{\text{RS}}^*$  value.

Empirically, we observe that the HPR performs the best when the messages cease to converge quickly to the BP-like fixed point (as in Figure 11 (Left)), which is consistent with the discussion of BP reinforcement in [67]. This regime can be found by fine-tuning the  $\pi$  and  $\lambda$ .

**Time evolution of  $\mathbf{x}^{\text{sol}}$ .** In Figures 12, 13 and 14, we show all of the values of  $m_{\text{init}}(\mathbf{x}_t^{\text{sol}})$  and the time to consensus  $T_{\text{eff}}(\mathbf{x}_t^{\text{sol}})$  under the majority rule, for all  $\mathbf{x}_t^{\text{sol}}$  from the trajectories of HPR runs. This shows that the algorithm not only finds configurations that converge of the desired kind, but also that it first finds those that converge a little bit less fast, sometimes with a lower initial magnetization. This trade-off is clearly visible on the plots for different values of  $p$  and  $d$ .

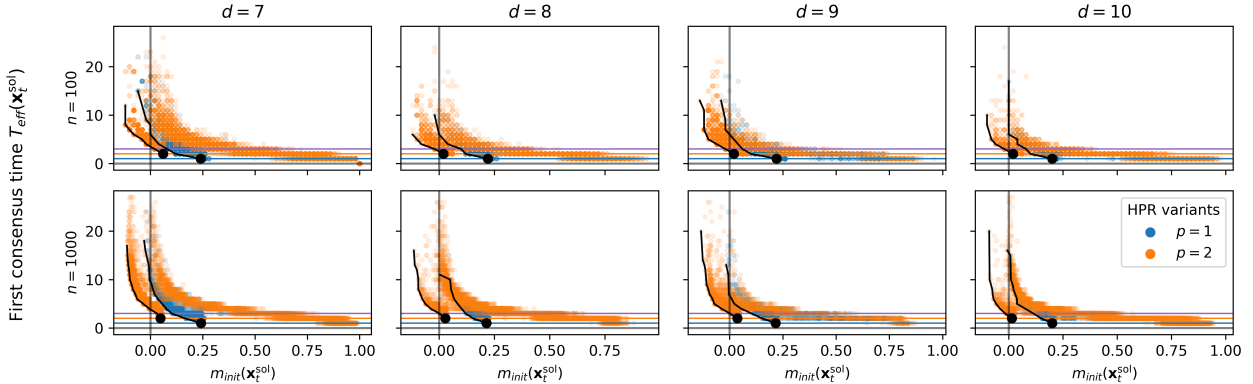


Figure 13: Similar to Figure 12 for  $d = 7, 8, 9, 10$ .

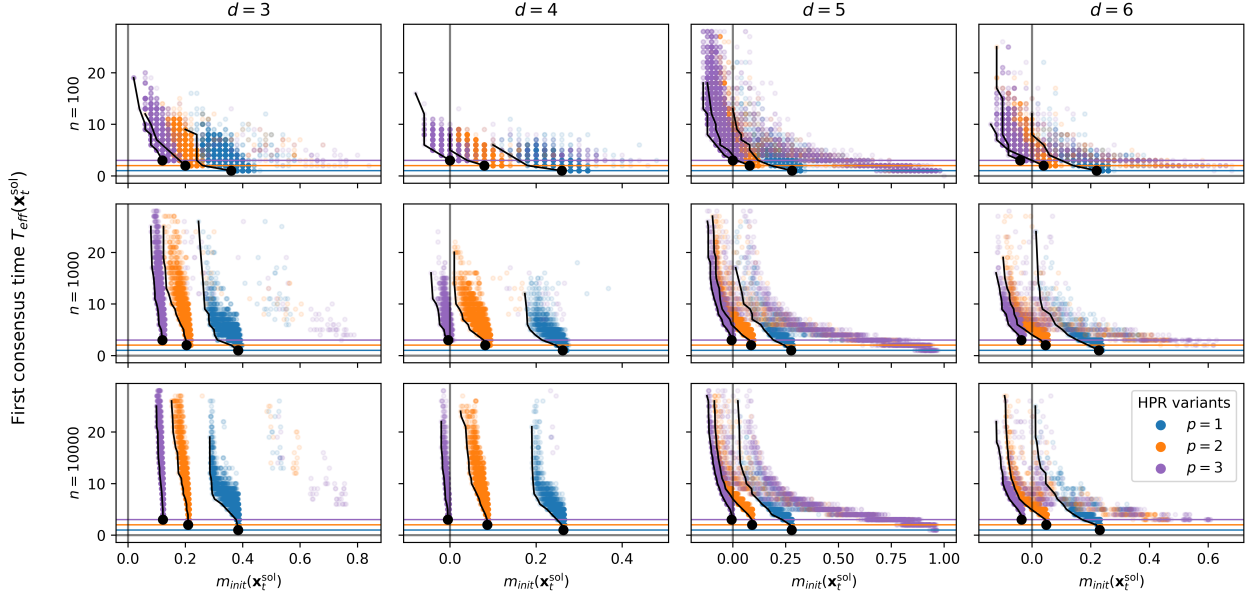


Figure 12: Values of  $m_{\text{init}}(\mathbf{x}_t^{\text{sol}})$  and the time to consensus  $T_{\text{eff}}(\mathbf{x}_t^{\text{sol}})$  under the majority rule, for all  $\mathbf{x}_t^{\text{sol}}$  from the trajectories of HPR runs with  $d = 3, 4, 5, 6$ . We exclude every  $\mathbf{x}_t^{\text{sol}}$  that failed to reach consensus within 28 timesteps. We ran the HPR for 10 random graphs and plot all results. The black lines are the lowest  $m_{\text{init}}$  for each  $T_{\text{eff}} > p$  with  $p = 1, 2, 3$  over the 10 runs and black dots indicate the best  $m_{\text{init}}$  for a given  $T_{\text{eff}} = p$ . Note that this reports different values than Table 3, where we reported the average best initialization.

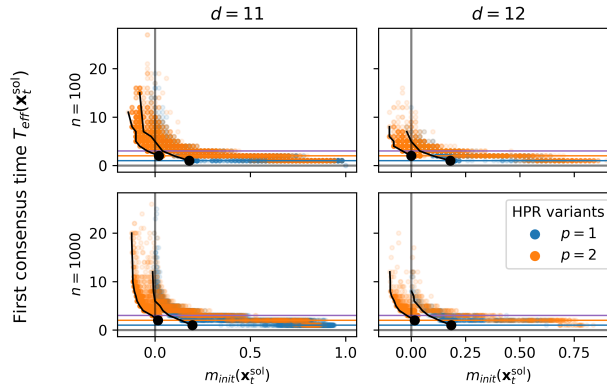


Figure 14: Similar to Figure 12 for  $d = 11, 12$ .

### C.3 Dynamic programming scheme for HPR

We show how dynamic programming significantly reduces the algorithmic complexity of Algorithm 1 for the HPR procedure. We repeat the general HPR message update equation here for convenience:

$$\chi_{\underline{x}_i, \underline{x}_j}^{i \rightarrow j} = \frac{1}{Z^{i \rightarrow j}} a(\underline{x}_i, \underline{x}_j) \sum_{\underline{x}_{\partial i \setminus j}} \mathcal{A}_i(\underline{x}_i, \underline{x}_{\partial i}) \prod_{k \in \partial i \setminus j} b_{x_k}^k \chi_{\underline{x}_k, \underline{x}_i}^{k \rightarrow i}. \quad (79)$$

The factor node  $\mathcal{A}_i(\underline{x}_i, \underline{x}_{\partial i})$  depends on the neighboring trajectories of node  $i$  only via the dynamical rule  $f_i(\underline{x}_i, \underline{x}_{\partial i})$ . In the following, we consider a dynamical rule that depends only on the sum of the neighboring values:  $f_i(\underline{x}_i, \underline{x}_{\partial i}) = f_i(\underline{x}_i, \underline{x}_j, \varrho_{\partial i \setminus j})$ , where  $\varrho_{\partial i \setminus j} = \sum_{k \in \partial i \setminus j} x_k$ . This is the case for the majority dynamics

rule (1) from Section 4. Thus, we can write the majority dynamics rule as:

$$f_i(x_i, x_j, \underline{\varrho}_{\partial i \setminus j}) = \text{sign} \left( 2(x_j + \underline{\varrho}_{\partial i \setminus j})) + x_i \right). \quad (80)$$

Hence, for the factor node  $\mathcal{A}_i$  we can write

$$\mathcal{A}_i(\underline{x}_i, \underline{x}_{\partial i}) = \mathcal{A}_i(\underline{x}_i, \underline{x}_j, \underline{\varrho}_{\partial i \setminus j}), \quad (81)$$

where  $\underline{\varrho}_{\partial i \setminus j}$  is the *sum trajectory*  $(\varrho_{\partial i \setminus j}^1, \dots, \varrho_{\partial i \setminus j}^T)$  with  $\varrho_{\partial i \setminus j}^t = \sum_{k \in \partial i \setminus j} x_k^t$ . This is useful because a large number of trajectory combinations correspond to the same value of  $\underline{\varrho}_{\partial i \setminus j}$  and we can rewrite the message update (79) as

$$\chi_{\underline{x}_i, \underline{x}_j}^{i \rightarrow j} = \frac{1}{Z^{i \rightarrow j}} a(\underline{x}_i, \underline{x}_j) \sum_{\underline{\varrho}_{\partial i \setminus j}} \mathcal{A}_i(\underline{x}_i, \underline{x}_j, \underline{\varrho}_{\partial i \setminus j}) \underbrace{\sum_{\underline{x}_{\partial i \setminus j}} \mathbf{1} \left[ \sum_{k \in \partial i \setminus j} x_k = \underline{\varrho}_{\partial i \setminus j} \right]}_{L_{\tilde{D}=d(i)-1}(\underline{x}_i, \underline{\varrho}_{\partial i \setminus j})} \prod_{k \in \partial i \setminus j} b_{x_k^1}^{k_1} \chi_{\underline{x}_k, \underline{x}_i}^{k \rightarrow i}, \quad (82)$$

where  $L_{\tilde{D}}(\underline{x}_i, \underline{\varrho}_{\partial i \setminus j})$  can be computed recursively. We start with  $\tilde{D} = 1$ , when

$$L_1(\underline{x}_i, \underline{\varrho}_1) = b_{x_{k_1}^1}^{k_1} \chi_{\underline{x}_{k_1} = \underline{\varrho}_1, \underline{x}_i}^{k_1 \rightarrow i}, \quad (83)$$

for some  $k_1 \in \partial i \setminus j$ . Indeed, we aim to obtain the sum of the products of the biased neighboring messages,  $L_{\tilde{D}=d(i)-1}(\underline{x}_i, \underline{\varrho}_{\partial i \setminus j})$ , but we start with just one message, and hence for the sum trajectory of neighboring “nodes” we have directly  $\underline{\varrho}_1 = \underline{x}_{k_1}$ . Then, we add neighboring messages according to

$$L_{\tilde{D}}(\underline{x}_i, \underline{\varrho}_{\tilde{D}}) = \sum_{\underline{x}_{k_{\tilde{D}}}} \sum_{\underline{\varrho}_{\tilde{D}-1}} \mathbf{1} \left[ x_{k_{\tilde{D}}} + \underline{\varrho}_{\tilde{D}-1} = \underline{\varrho}_{\tilde{D}} \right] L_{\tilde{D}-1}(\underline{x}_i, \underline{\varrho}_{\tilde{D}-1}) b_{x_{k_{\tilde{D}}}^1}^{k_{\tilde{D}}} \chi_{\underline{x}_{k_{\tilde{D}}}, \underline{x}_i}^{k_{\tilde{D}} \rightarrow i}. \quad (84)$$

In this way, we use all neighboring nodes in  $\partial i \setminus j$  uniquely for the *final*  $\tilde{D} = d(i) - 1$ . Note that we use (84) to obtain  $L_{\tilde{D}}(\underline{x}_i, \underline{\varrho}_{\tilde{D}})$  for each combination of  $\underline{\varrho}_{\tilde{D}}$ .

In the case of  $d$ -RRGs the final value of  $D = d(i) - 1$  is the same for every node,  $d(i) = d \forall i \in V$ . Hence, we need to compute and keep only the final values  $L_{\tilde{D}=d-1}(\underline{x}_i, \underline{\varrho}_{\partial i \setminus j})$  for each message (see Algorithm 2 for the algorithmic procedure in this case). If the node degree varies, we can use the same dynamic procedure as described here, but we need to store  $L_{\tilde{D}=d(i)-1}(\underline{x}_i, \underline{\varrho}_{\partial i \setminus j})$  for the given range of node degrees.

The new update scheme

$$\chi_{\underline{x}_i, \underline{x}_j}^{i \rightarrow j} = \frac{1}{Z^{i \rightarrow j}} a(\underline{x}_i, \underline{x}_j) \sum_{\underline{\varrho}_{\partial i \setminus j}} \mathcal{A}_i(\underline{x}_i, \underline{x}_j, \underline{\varrho}_{\partial i \setminus j}) L_{d(i)-1}(\underline{x}_i, \underline{\varrho}_{\partial i \setminus j}) \quad (85)$$

is summing over  $d(i)^{p+c}$  terms (the sum of  $d(i) - 1$  binary values can result in  $d(i)$  outcomes) instead of  $2^{(d-1)(p+c)}$  terms. Hence, the exponential dependence on  $d(i)$  is removed. Naturally, a similar dynamic programming scheme can also be devised for other permutation-symmetric dynamical rules.

---

**Algorithm 2** History Passing Reinforcement – dynamic programming for majority dynamics on  $d$ -RRGs (factor graph  $(G, S, F, \{\Xi_k\}, \{\lambda_k\}, p, c)$ , steps threshold  $T_{\max}$ , damping  $\varepsilon$ , hyperparameters:  $\pi, \gamma$ )

---

Initialize uniformly at random biases  $b_{x_i}^i$  and messages  $\chi_{\underline{x}_i, \underline{x}_j}^{i \rightarrow j}$  on the factor graph and normalize them.  
 Initialize the sum trajectory values  $\{\underline{\varrho}_1\}$  with single node trajectory values  $\underline{x} \in S^{p+c}$ , as  $\underline{\varrho}_1 = \underline{x}$ .  
 $t \leftarrow 0$   
**while**  $t \leq T_{\max}$  **do**  
 Compute  $L_1(\underline{x}_i, \underline{\varrho}_1)$  for all  $\{\underline{x}_i\}$  and  $\{\underline{\varrho}_1\}$  according to (83).  
**for**  $\tilde{D} \in \{2, \dots, d-1\}$  **do**  
 For all  $\{\underline{\varrho}_{\tilde{D}}\}$  and  $\{\underline{x}_i\}$  compute  $L_{\tilde{D}}(\underline{x}_i, \underline{\varrho}_{\tilde{D}})$  according to (84).  
**end for**  
 Update all the messages  $\chi_{\underline{x}_i, \underline{x}_j}^{i \rightarrow j}$  according to (85) with damping  $\varepsilon$  (29).  
 Compute the marginals  $\mu_{x_i^1=s}^i$  from eq. (25).  
 Update each bias independently according to (24) with probability  $p(t)$  (27).  
 Obtain new trial solution  $\mathbf{x}_t^{\text{sol}}$  using (28).  
 $t \leftarrow t + 1$   
**end while**  
**return**  $\mathbf{x}_t^{\text{sol}}$  with lowest initial magnetization and which is a solution.

---

#### C.4 HPR results for small $n$

In addition to the experiments in the main text, we add HPR results for small  $n = 100$  and  $n = 1000$  in Tables 5 and 6. In Table 7 we provide additional results for  $n = \{100, 1000\}$  for  $p \in [7, 14]$ .

$p$	1	2	3		
$d$				4	5
3	0.3720	0.2080	0.1200	0.1467	0.1313
4	0.2640	0.0900	0.0000	<b>-0.006</b>	<b>-0.019</b>
5	0.2820	0.0800	0.0000	<b>-0.015</b>	<b>-0.030</b>
6	0.2360	0.0511	<b>-0.040</b>	<b>-0.044</b>	<b>-0.048</b>

Table 5: HPR results for  $n = 100$  for  $p = 1, 2, 3$  on  $d = 3, 4, 5, 6$  regular graphs. We sampled 10 graphs together with random initializations and report the average over the minimum  $m_{\text{init}}$  that reaches consensus in exactly  $p$  steps from each run. For  $p = 4, 5$  we select the minimal  $m_{\text{init}}$  over all runs of the HPR for  $p = \{1, 2, 3\}$  when they were encountered during the runtime.

$p$	1	2	3		
$d$				4	5
3	0.3840	0.2072	0.1200	0.1200	0.1195
4	0.2622	0.0846	<b>-0.003</b>	0.0027	0.0019
5	0.2778	0.0892	<b>-0.005</b>	<b>-0.008</b>	<b>-0.009</b>
6	0.2292	0.0488	<b>-0.036</b>	<b>-0.028</b>	<b>-0.030</b>

Table 6: HPR results for  $n = 1000$  for  $p = 1, 2, 3$  on  $d = 3, 4, 5, 6$  regular graphs. We sampled 10 graphs together with random initializations and report the average over the minimum  $m_{\text{init}}$  from each run. For  $p = 4, 5$  we select the minimal  $m_{\text{init}}$  over all runs of the HPR for  $p = \{1, 2, 3\}$  when they were encountered during the runtime.

		n			
		100		1000	
p	d	1	2	1	2
7	0.240	0.060		0.2428	0.1093
8	0.220	0.024		0.2146	0.0284
9	0.220	0.022		0.2166	0.0360
10	0.200	0.022		0.2003	0.0170
11	0.186	0.020		0.1960	0.0170
12	0.180	0.002		0.1847	0.0166
13	0.180	0.020		0.1871	0.0180
14	0.172	0.006		0.1740	0.0102

Table 7: HPR results for  $n = 100$  and  $n = 1000$  for  $p = 1, 2$  on  $d = \{7, 8, 9, 10, 11, 12, 13, 14\}$  random regular graphs. We sampled 10 graphs together with random initializations and report the average over the minimum  $m_{\text{init}}$  from each run.

### C.5 Parameter values for HPR on $d$ -RRGs with majority always-stay dynamics

The complete list of hyperparameters for the HPR experiments is shown below in Table 8, used for generating the HPR results in Tables 3, 6 and 7. For all experiments we set  $\gamma = 0.1$  and  $T_{\text{max}} = 10^4$ . Furthermore, the result files are available in the accompanying code.

d	p	n	bias	$\pi$	dampening	$\varepsilon$	temp	$\lambda_{\text{init}}$
			1	2	3	4	5	
3	1	100	0.25	0.20	25			
		1000	0.25	0.20	25			
		10000	0.25	0.20	25			
	2	100	0.25	0.20	18			
		1000	0.25	0.20	18			
		10000	0.25	0.20	18			
	3	100	0.30	0.20	25			
		1000	0.30	0.20	25			
		10000	0.30	0.20	25			
4	1	100	0.30	0.40	25			
		1000	0.30	0.40	25			
		10000	0.30	0.40	25			
	2	100	0.20	0.10	25			
		1000	0.20	0.10	25			
		10000	0.20	0.10	25			
	3	100	0.30	0.40	20			
		1000	0.30	0.40	20			
		10000	0.30	0.40	20			
5	1	100	0.30	0.40	25			
		1000	0.30	0.40	25			
		10000	0.30	0.40	25			
	2	100	0.20	0.10	25			
		1000	0.20	0.10	25			
		10000	0.20	0.10	25			
	3	100	0.30	0.15	19			
		1000	0.30	0.15	17			
		10000	0.30	0.15	17			
6	1	100	0.20	0.40	25			
		1000	0.20	0.40	25			
		10000	0.20	0.40	25			
	2	100	0.20	0.10	20			
		1000	0.20	0.10	20			
		10000	0.20	0.10	20			
	3	100	0.20	0.15	15			
		1000	0.20	0.15	15			

		10000	0.20	0.15	15
7	1	100	0.15	0.05	30
		1000	0.15	0.05	30
		10000	0.15	0.05	30
	2	100	0.15	0.05	30
		1000	0.15	0.05	30
		10000	0.15	0.05	30
8	1	100	0.20	0.15	15
		1000	0.20	0.15	15
		10000	0.20	0.15	15
	2	100	0.20	0.15	15
		1000	0.20	0.15	15
		10000	0.20	0.15	15
9	1	100	0.20	0.15	15
		1000	0.20	0.15	15
		10000	0.20	0.15	15
	2	100	0.15	0.05	17
		1000	0.15	0.05	17
		10000	0.15	0.05	17
10	1	100	0.20	0.15	10
		1000	0.20	0.15	10
	2	100	0.20	0.15	10
		1000	0.20	0.15	10
	11	100	0.20	0.15	10
		1000	0.20	0.15	10
11	2	100	0.15	0.05	25
		1000	0.15	0.05	25
	12	100	0.20	0.15	10
		1000	0.20	0.15	10
	12	100	0.10	0.10	15
		1000	0.10	0.10	15
13	1	100	0.15	0.05	25
		1000	0.15	0.05	25
	2	100	0.10	0.10	15
		1000	0.10	0.10	15
	14	100	0.20	0.15	10
		1000	0.20	0.15	10
14	2	100	0.10	0.10	15
		1000	0.10	0.10	15

Table 8: HPR hyperparameters for all the tested settings.

## D Simulated Annealing

In this section, we present the simulated annealing (SA) [39] procedure for enhancing consensus in our setting. That is, we use SA to obtain initializations of  $d$ -RRGs leading to all-ones attractor via majority dynamics while minimizing  $m_{\text{init}}$ . We compare the results of this widely used Markov Chain Monte Carlo (MCMC) optimization method [47, 32, 39] with the HPR algorithm in Section 5.

We define the energy function

$$E(\mathbf{x}) = anm_{\text{init}}(\mathbf{x}) - bnm_{\text{attr}}(\mathbf{x}), \quad (86)$$

which we aim to minimize.  $n$  is the number of nodes and we introduce two parameters  $a$  and  $b$ , which are interpretable as two inverse temperatures. The energy function (86) aligns with our goal of finding initializations where minority becomes majority via majority dynamics: its minima are the states that minimize  $m_{\text{init}}$  and maximize  $m_{\text{attr}}$  (recall that homogeneous attractor corresponds to  $m_{\text{attr}} = 1$ ). Note that the energy is a function only of the graph initialization because of the deterministic dynamics:  $E(\mathbf{x}) = anm(\mathbf{x}^1) - bnm(\mathbf{x}^{p+1}) = anm(\mathbf{x}^1) - bnm(F^{op}(\mathbf{x}^1)) = E(\mathbf{x}^1)$ . This is convenient because the combinatorial space to search is  $S^n$  instead of  $S^{n(p+1)}$ . We construct the Boltzmann probability measure on graph configurations  $\mathbf{x}^1 = \mathbf{x} \in S^n$

$$P(\mathbf{x}) = \frac{1}{Z} e^{-E(\mathbf{x})}. \quad (87)$$

As we ‘cool’ the system, i.e. we increase the inverse temperatures  $a \sim b \rightarrow \infty$ , the measure (87) concentrates

on the ground-states of the energy (86). Hence, if we can sample from this probability distribution at lower and lower temperatures, we obtain (approximate) ground-states of the energy (86). The SA procedure achieves this by performing Metropolis-Hastings (MH) steps with increasing inverse temperatures. This MCMC process is defined by the transition rates based on the ratio  $P(\mathbf{x}')/P(\mathbf{x}) = e^{-(E(\mathbf{x}')-E(\mathbf{x}))}$ . If the probability of state  $\mathbf{x}'$  is higher than the probability of  $\mathbf{x}$  (hence  $E(\mathbf{x}') < E(\mathbf{x})$ ) the MH step always accepts the new state  $\mathbf{x}'$ . If the state  $\mathbf{x}'$  is less probable, MH accepts it only with probability  $e^{-(E(\mathbf{x}')-E(\mathbf{x}))}$ . Thus, the transition rates from state  $\mathbf{x}$  to  $\mathbf{x}'$  is

$$p(\mathbf{x}'|\mathbf{x}) = \min \left( 1, e^{-(E(\mathbf{x}')-E(\mathbf{x}))} \right), \quad (88)$$

which satisfy the detailed balance condition with the equilibrium distribution given by (87). Moreover, by defining the transition rates by a ratio of probabilities (87) we get rid of the hard to compute partition function  $Z$ .

A slow cooling is essential for a good performance of the SA procedure. We adopt the following cooling schedule. We start with inverse temperature values  $a_i, b_i$  and increase them with the same rate  $\alpha > 1$ , so that  $a^{t+1} = \alpha a^t$  (and equivalently for  $b^{t+1}$ ) until we reach the final inverse temperature values  $a_f, b_f$ . We chose the numerical values of  $\{a_i, b_i, a_f, b_f, \alpha\}$  based on empirical observations of the performance of the SA algorithm in our setting. The precise values used for the results in Table 3 are summarized in Table 9. We initialize the binary node values uniformly at random and the trial state  $\mathbf{x}'$  is created by choosing one node (uniformly at random) and flipping its sign. The entire SA procedure is summarized in Algorithm 3.

---

**Algorithm 3** Simulated Annealing ( $G, S, F, E, \alpha, a_i, a_f, b_i, b_f, T_{\max}$ )

---

Initialize graph configuration  $\mathbf{x}^{\text{sol}} \in S^n$  uniformly at random and compute the energy  $E(\mathbf{x}^{\text{sol}})$ , with  $a = a_i$ ,  $b = b_i$ , according to (86).

$t \leftarrow 0$

**while**  $\mathbf{x}^{\text{sol}}$  is not a solution **and**  $t \leq T_{\max}$  **do**

    Choose  $i \in V$  uniformly at random and take  $\mathbf{x}'_i = -\mathbf{x}^{\text{sol}}_i$ ,  $\mathbf{x}'_j = \mathbf{x}^{\text{sol}}_j$  for all  $j \in V \setminus i$ .

$\Delta E \leftarrow E(\mathbf{x}') - E(\mathbf{x}^{\text{sol}})$ .

$r \leftarrow \text{Random}(0, 1)$

**if**  $r \leq \min(1, e^{-\Delta E})$  **then**

$\mathbf{x}^{\text{sol}} \leftarrow \mathbf{x}'$

**end if**

**if**  $a < a_f$  **then**

$a \leftarrow \alpha a$

**end if**

**if**  $b < b_f$  **then**

$b \leftarrow \alpha b$

**end if**

$t \leftarrow t + 1$

**end while**

---

$d$	$a_i, b_i, a_f, b_f$
3	0.015, 0.01, 4, 6
4	0.015, 0.01, 4, 6
5	0.015, 0.01, 4, 6
6	0.015, 0.01, 4.5, 5

Table 9: Parameter values used in the computation of the results presented in Table 3 for  $p = 3$ . The cooling rate was set to  $\alpha = 1.0005$ , and we used  $T_{\max} = 2n^3$  for the maximum SA steps threshold.

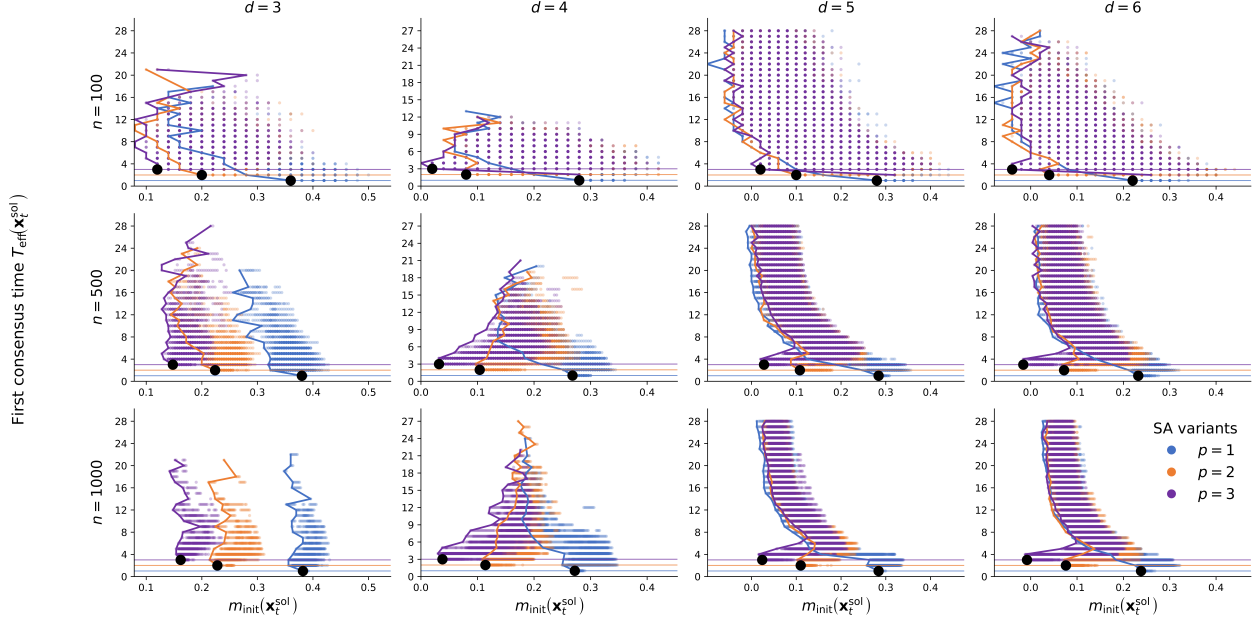


Figure 15: Values of  $m_{\text{init}}(\mathbf{x}_t^{\text{sol}})$  and the time to consensus  $T_{\text{eff}}(\mathbf{x}_t^{\text{sol}})$  under the majority rule, for all  $\mathbf{x}_t^{\text{sol}}$  from the trajectories of SA runs with  $d = 3, 4, 5, 6$ . We exclude every  $\mathbf{x}_t^{\text{sol}}$  that failed to reach consensus within 28 time-steps. To avoid memory issues during the long runs of the SA procedure we plot the following combination of the SA runs. We ran the SA until we reach a solution ( $T_{\text{eff}} = p$ ) for 10 random graphs and plot every  $10^4$ th  $(m_{\text{init}}(\mathbf{x}_t^{\text{sol}}), T_{\text{eff}}(\mathbf{x}_t^{\text{sol}}))$  pair. And we ran the SA for another 10 random graphs for  $10^7$  time-steps and plot all  $(m_{\text{init}}(\mathbf{x}_t^{\text{sol}}), T_{\text{eff}}(\mathbf{x}_t^{\text{sol}}))$  pairs without reaching the solution. This allows us to resolve the early-stage behavior in detail while also capturing the final magnetization values reached, where  $m_{\text{init}}(\mathbf{x}_t^{\text{sol}})$  fluctuates only weakly around its final value. The black lines are the lowest  $m_{\text{init}}$  for each  $T_{\text{eff}} > p$  with  $p = 1, 2, 3$  over all runs and black dots indicate the best  $m_{\text{init}}$  for a given  $T_{\text{eff}} = p$ . Note that this figure reports different values than Table 3, where we reported the average best initialization. The hyperparameter values are  $a_i = 0.015$ ,  $b_i = 0.01$ ,  $a_f = 4.5$  and  $b_f = 5$ , except for the case  $d = 3$ ,  $n = 1000$  where  $b_f = 6$  was used. The cooling rate was set to  $\alpha = 1.0005$ , and for the maximum SA steps threshold we used  $T_{\text{max}} = n^3$  and  $T_{\text{max}} = 10^7$ .

We note that the behavior of the  $m_{\text{init}}(\mathbf{x}_t^{\text{sol}})$  trajectories during the SA run depicted in Figure 15 depends on the chosen cooling mechanism. In addition, their behavior in finding solutions with  $T_{\text{eff}}(\mathbf{x}_t^{\text{sol}}) > p$  differs somewhat from that of the HPR trajectories shown in Figure 12. For instance, the increase in the initial magnetization observed for  $p < T_{\text{eff}}(\mathbf{x}_t^{\text{sol}}) < 12$  in the cases  $p = 3$ ,  $d = 5, 6$ , and  $n = 500, 1000$  might be attributed to the fact that the temperature regime where the term in  $a$  is better optimized than the term in  $b$  does not persist long enough to generate these solutions. Furthermore, the solid lines corresponding to different values of  $p$  tend to collapse onto a single curve at large  $T_{\text{eff}}(\mathbf{x}_t^{\text{sol}})$ . This behavior may stem from the structure of the energy function (86) and the chosen cooling parameters: the first term is identical for all  $p$ , while the second term exerts a similar influence on the magnetization at high  $T_{\text{eff}}(\mathbf{x}_t^{\text{sol}})$  for  $p = 1, 2, 3$ . We did not investigate these effects further, as this cooling regime empirically proved effective for finding solutions with  $T_{\text{eff}}(\mathbf{x}_t^{\text{sol}}) \leq p$ , which was our primary focus.